Journal of Virology

Immunology | Full-Length Text

3β-hydroxysteroid-Δ24 reductase dampens anti-viral innate immune responses by targeting K27 ubiquitination of MAVS and STING

Qian Liu,[1] Shengwen Chen,[1] Renyun Tian,[1] Binbin Xue,[1] Huiyi Li,[1] Mengmeng Guo,[1] Shun Liu,[1] Ming Yan,[1] Ruina You,[1] Luoling Wang,[1] Di Yang,[1] Mengyu Wan,[1] Haizhen Zhu[1,2,3]

AUTHOR AFFILIATIONS See affiliation list on p. 20.

ABSTRACT The mechanism by which lipid metabolism regulates innate immunity is unknown. Here, we report that the key enzyme in cholesterol synthesis, 3β-hydroxysteroid-Δ24 reductase (DHCR24), is inhibited by viral infection. DHCR24 deficiency significantly promotes interferon production and interferon-stimulated gene expression. Inhibition of DHCR24 enzyme activity or the addition of the precursor 24-dehydrocholesterol (24-DHC) can augment innate immunity. Mechanistically, DHCR24 interacts with MAVS or STING, and DHCR24 impairs K27-linked ubiquitination of MAVS mediated by TRIM21 and K27-linked ubiquitination of STING mediated by AMFR, blocking the activation of MAVS and STING, respectively. Collectively, DHCR24 plays a negative role in regulating innate immune responses that may be targeted to improve immunity.

IMPORTANCE The precise regulation of the innate immune response is essential for the maintenance of homeostasis. MAVS and STING play key roles in immune signaling pathways activated by RNA and DNA viruses, respectively. Here, we showed that DHCR24 impaired the antiviral response by targeting MAVS and STING. Notably, DHCR24 interacts with MAVS and STING and inhibits TRIM21-triggered K27-linked ubiquitination of MAVS and AMFR-triggered K27-linked ubiquitination of STING, restraining the activation of MAVS and STING, respectively. Together, this study elucidates how one cholesterol key enzyme orchestrates two antiviral signal transduction pathways.

KEYWORDS DHCR24, innate immunity, cholesterol metabolism, IFN, MAVS, STING, TRIM21, AMFR, viral infection

The crosstalk between innate immunity and cholesterol homeostasis is instrumental for maintaining a normal physiological state (1, 2). Cholesterol metabolism-related proteins and products are related to innate immunity. Cholesterol-25-hydroxylase (CH25H) is a broadly antiviral interferon-stimulated gene (ISG) that inhibits the replication of various enveloped viruses by converting cholesterol to 25-hydroxycholesterol (25HC) (3). Moreover, the restriction of cholesterol biosynthesis spontaneously increases interferon (IFN) production in a STING-dependent manner (4). Upon viral infection, the cholesterol biosynthesis enzyme 7-dehydrocholesterol reductase (DHCR7) is reduced in macrophages and then the precursor 7-dehydrocholesterol (7-DHC) accumulates, which is accompanied by the activation of AKT3-IRF3, enhancing IFN-β production (5). Tim-4 reprograms cholesterol metabolism to suppress antiviral innate immunity by disturbing the Insig1-SCAP interaction in macrophages (6). Cumulatively, proper cholesterol metabolism is important for the host to maintain homeostasis against viral infection.

Nucleic acid sensing is a cornerstone of host defense. Retinoic-acid-inducible gene I (RIG-I)-like receptors (RLRs), such as RIG-I and MDA5, detect foreign and host RNA

Editor Anna Ruth Cliffe, University of Virginia, Charlottesville, Virginia, USA

Address correspondence to Haizhen Zhu, hy0206218@hainmc.edu.cn.

The authors declare no conflict of interest.

See the funding table on p. 21.

Received 27 September 2023
Accepted 2 November 2023
Published 30 November 2023

to trigger acute inflammation by activating the downstream-signaling axis (7–9). Upon sensing viral RNA, RIG-I and MDA5 undergo conformational changes and interact with MAVS (also known as IPS1, VISA, and Cardif). Once activated, MAVS CARD rapidly forms prion-like aggregates, which convert other MAVS on the mitochondrial outer membrane into prion-like aggregates (10). This aggregation process enables MAVS to activate the TANK-binding kinase 1 (TBK1). Then, activated TBK1 phosphorylates IFN regulatory factor 3 (IRF3), which translocates to the nucleus and promotes the transcription of type I and III IFNs (11–14). Although MAVS is orchestrated in a variety of ways in innate immunity, the relationship between cholesterol metabolism and MAVS is unknown.

The cyclic GMP-AMP (cGAMP) synthase (cGAS)-STING (also known as MITA, ERIS, and MPYS) pathway is a major pathway mediating immune defense against DNA virus infection (15). Upon DNA binding, cGAS converts ATP and GTP into the noncanonical cyclic dinucleotide cGAMP to bind and activate STING which anchors as a homodimer within the endoplasmic reticulum (ER) membrane in the resting state. The binding of cGAMP triggers STING trafficking from the ER to the ER-Golgi intermediate compartments and the Golgi apparatus, as a platform to recruit TBK1 and IRF3, which leads to oligomerization and downstream activation of IRF3-dependent IFN responses (16–19). Although it was reported that cholesterol levels directly influence the ability of STING to transduce signals to TBK1 (4), little is known about whether cholesterol metabolism-related products or enzymes are involved in the regulation of STING.

3β-hydroxysteroid-Δ24 reductase (DHCR24) is an enzyme that catalyzes 24-DHC to cholesterol, a final step in cholesterol synthesis (20–22). DHCR24 is involved in various physiological and pathological aspects, including apoptosis (23–25), oncogenic and oxidative stress (26), and tumor immune surveillance (27, 28). Missense mutations in DHCR24, which result in diminished protein activity, can lead to a rare autosomal recessive disorder, desmosterolosis, whereby patients have elevated desmosterol and lowered cholesterol, resulting in multiple congenital anomalies (21, 29). However, to date, whether and how DHCR24 modulates the host innate immunity remains unclear.

Here, our results show an unanticipated role for DHCR24. Silencing DHCR24 or adding the DHCR24 inhibitor-U18666A upregulated the expression of *IFN-β*, *IL28A*, *IL29*, *ISG15*, and *MX1*, which is consistent with the significant clearance of vesicular stomatitis virus (VSV) and Herpes simplex virus (HSV). Moreover, DHCR24 inhibits the IRF3-dependent innate immune response. Mechanistically, DHCR24 interacts with MAVS or STING and inhibits K27-linked ubiquitination of MAVS regulated by TRIM21 and K27-linked ubiquitination of STING mediated by autocrine motility factor receptor (AMFR), thus blocking the recruitment of TBK1 to MAVS or STING and subsequently inhibiting innate immune responses to viral infection. This study reveals a novel role of DHCR24 in innate immunity and establishes a new relationship between cholesterol metabolism and innate immunity.

RESULTS

DHCR24 negatively regulates innate immune responses to viral infection

To understand how cholesterol metabolism in the liver is linked to innate immune signals, we used RNA deep sequencing to analyze the gene profiles in HLCZ01 cells (30), with or without VSV infection (Table S1). We focused on enzymes associated with various metabolites and ultimately identified DHCR24, an enzyme involved in cholesterol metabolism that was downregulated upon VSV infection in HLCZ01 cells (Fig. 1A) but whose function in innate immunity is unknown. We first verified the results of RNA-seq. HLCZ01 cells were treated with the 3′ untranslated region of HCV RNA (HCV 3′ UTR), high-molecular weight poly(I:C), VSV, Newcastle disease virus (NDV) or HSV, which substantially reduced *DHCR24* mRNA levels (Fig. 1B). To detect the effect of DHCR24 on the innate immune response, we transfected HEK293T cells with an IFN-β luciferase reporter plasmid and then treated the cells with VSV. DHCR24 potently inhibited VSV-triggered IFN-β luciferase reporter activation in a dose-dependent manner (Fig. 1C). Accordingly, VSV-induced interferon stimulated response element (ISRE) luciferase

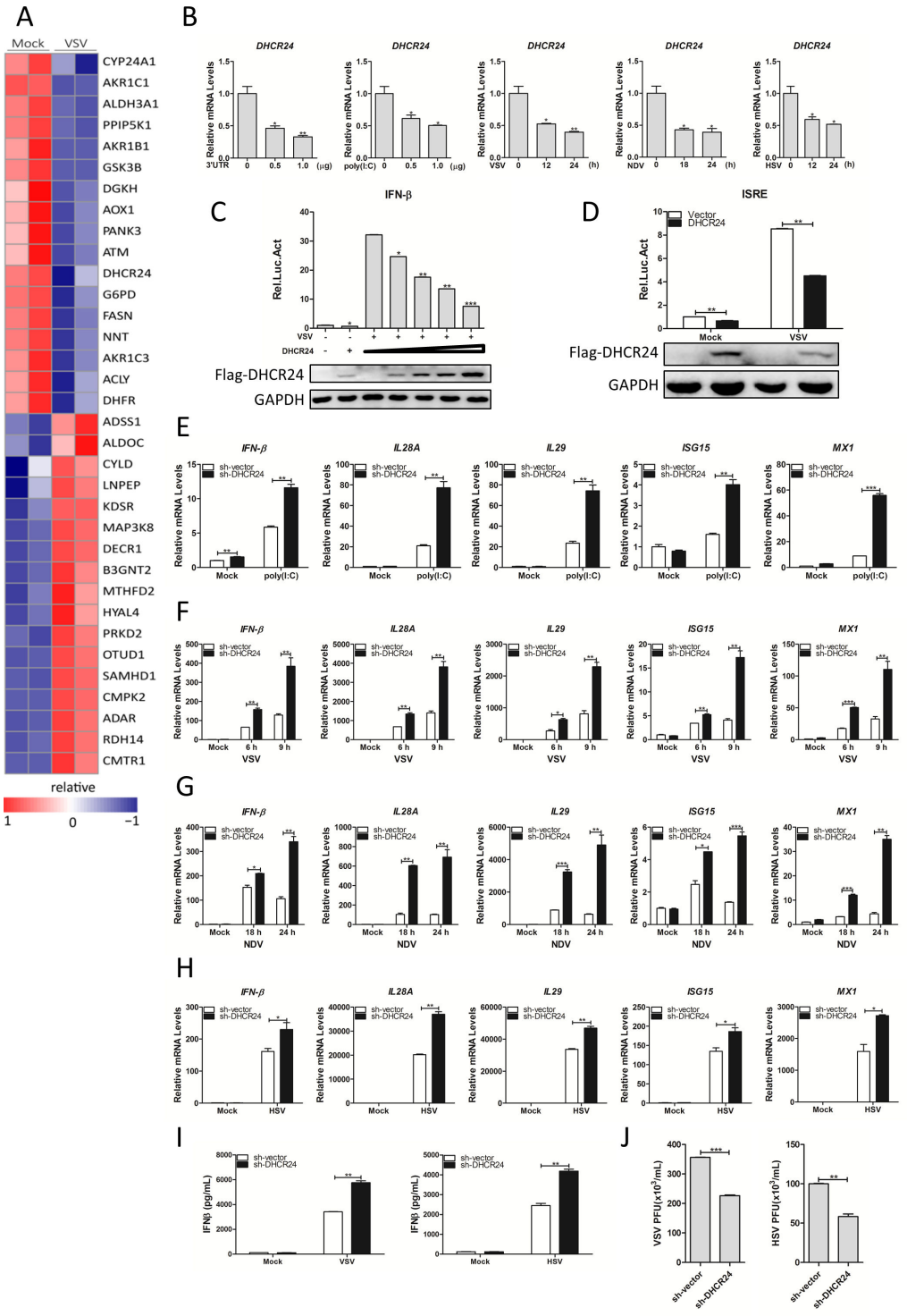

FIG 1 DHCR24 negatively regulates the innate immune responses to viral infection. (A) HLCZ01 cells were treated with VSV (multiplicity of infection [MOI] = 0.01) for 12 h before RNA extraction, and RNA-Seq was performed. (B) HLCZ01 cells were transfected with 0.5 or 1.0 μg of HCV 3′ UTR RNA or high molecular weight (HMW) poly(I:C) for 18 h or infected with VSV (MOI = 0.05), NDV (MOI = 0.05), and HSV (MOI = 0.05) for the indicated times. DHCR24 mRNAs were measured by quantitative real-time PCR (qRT-PCR) and normalized with GAPDH. (C) HEK293T cells were transfected with an IFN-β promoter reporter (0.1 μg) and an increased amount of DHCR24 expression plasmid. 12 h after transfection, the cells were infected with VSV (MOI = 0.01) or left untreated. Luciferase assays were performed 12 h after infection. (D) HEK293T cells were transfected with an ISRE promoter reporter (0.1 μg) and DHCR24 expression plasmid (0.5 μg). 12 h after transfection, the cells were infected

(Continued on next page)

FIG 1 (Continued)

with VSV (MOI = 0.01) or left untreated. Luciferase assays were performed 12 h after infection. (E) Control cells or stable DHCR24-silenced Huh7 cells were transfected with 1.0 µg of HMW poly(I:C) for 12 h. IFN-β, IL-28A, IL-29, ISG15, and MX1 mRNAs were measured by qRT-PCR and normalized with GAPDH. (F and G) Control cells or stable DHCR24-silenced Huh7 cells were infected with VSV (MOI = 0.5) (F) or NDV (MOI = 0.01) (G) for the indicated times. IFN-β, IL-28A, IL-29, ISG15, and MX1 mRNAs were measured by qRT-PCR and normalized with GAPDH. (H) Control cells or stable DHCR24-silenced HLCZ01 cells were infected with HSV (MOI = 0.01) for 12 h. IFN-β, IL-28A, IL-29, ISG15, and MX1 mRNAs were measured by qRT-PCR and normalized with GAPDH. (I) Control cells or stable DHCR24-silenced HLCZ01 cells were infected with VSV (MOI = 0.01) for 9 h or HSV (MOI = 0.01) for 12 h. IFN-β protein in the supernatant was examined by enzyme-linked immunosorbent assay (ELISA). (J) Control cells or stable DHCR24-silenced HLCZ01 cells were infected with VSV (MOI = 0.01) for 9 h or HSV (MOI = 0.01) for 12 h to check PFU by plaque assay. All experiments were repeated at least three times with consistent results. Bar graphs show the means "±" SD ($n = 3$). *$P < 0.05$, **$P < 0.01$, and ***$P < 0.001$.

reporter activity was markedly decreased by DHCR24 (Fig. 1D). Next, we used the lentiviral short hairpin RNA (shRNA) expression system to knock down DHCR24. As shown in Fig. 1E, DHCR24-silenced Huh7 cells showed much stronger induction of *IFN-β*, interleukin-28A (*IL-28A*), *IL-29*, *ISG15*, and *MX1* mRNA by poly(I:C). To identify the role of DHCR24 in viral infection, we used different RLR stimuli including VSV or NDV infection. Consistent with the results in RNA nucleic acid mimic-treated cells, the knockdown of DHCR24 markedly enhanced *IFN-β*, *IL-28A*, *IL-29*, *ISG15*, and *MX1* mRNA production (Fig. 1F and G), accompanied by decreased PFU of VSV (Fig. 1J). Finally, we used HSV, which activates the STING signaling, to infect HLCZ01 cells. Silencing DHCR24 potentiated the expression of IFNs and ISGs triggered by HSV infection and reduced HSV PFU (Fig. 1H and J). IFN-β protein levels in the supernatant were enhanced in DHCR24-silenced HLCZ01 cells upon VSV or HSV infection (Fig. 1I). Taken together, these data demonstrate that DHCR24 negatively regulates the innate immune response to various viral infections.

DHCR24 inhibits innate immunity in IRF3-dependent manner

Upon recognition of cytosolic RNA, RLR undergoes an ATP-dependent conformational change that facilitates MAVS oligomerization, which triggers TBK1 activation and subsequent IRF3 phosphorylation for IFN-β production (7, 10). To understand how DHCR24 regulates IFN production during RLR activation, we examined the phosphorylation of IRF3. Consistent with increased IFN-β expression, IRF3 phosphorylation was upregulated in DHCR24-silenced cells upon poly(I:C) stimulus and VSV infection (Fig. 2A and B). Conversely, overexpression of DHCR24 attenuated the activation of IRF3 triggered by VSV or HSV infection (Fig. 2C and D). To exclude cell specificity, we repeated the experiment in HEK293T cells and observed similar results (Fig. 2E and F). Moreover, consistent with previous report (31), knockdown of DHCR24 decreased HCV NS3 protein levels (Fig. 2G). Finally, to detect whether the function of DHCR24 in regulating innate immunity depends on IRF3, we knocked out IRF3 in A549 cells. Knocking out IRF3 abolished the induction of IFNs and ISGs by viral infection in DHCR24-silenced cells (Fig. 2H). Collectively, these data support that DHCR24 inhibits innate immunity in an IRF3-dependent manner.

The DHCR24 inhibitor U18666A positively regulates virus-triggered innate immune signaling

Because DHCR24 is an enzyme that catalyzes 24-DHC to cholesterol, we examined whether DHCR24 enzyme activity is required for its modulation of the innate immune response to viral infection. U18666A, an inhibitor of DHCR24, binds to DHCR24, causing a structural change in DHCR24 and subsequently inhibiting the catalytic activity of DHCR24 (Fig. 3A) (32, 33). Treatment with different doses of U18666A in Huh7 cells inhibited DHCR24, as the lower band of DHCR24 protein shifted to the upper band after treatment with U18666A (Fig. 3B). We also validated that U18666A did not produce significant cytotoxicity or influence cell proliferation when the highest dose of U18666A

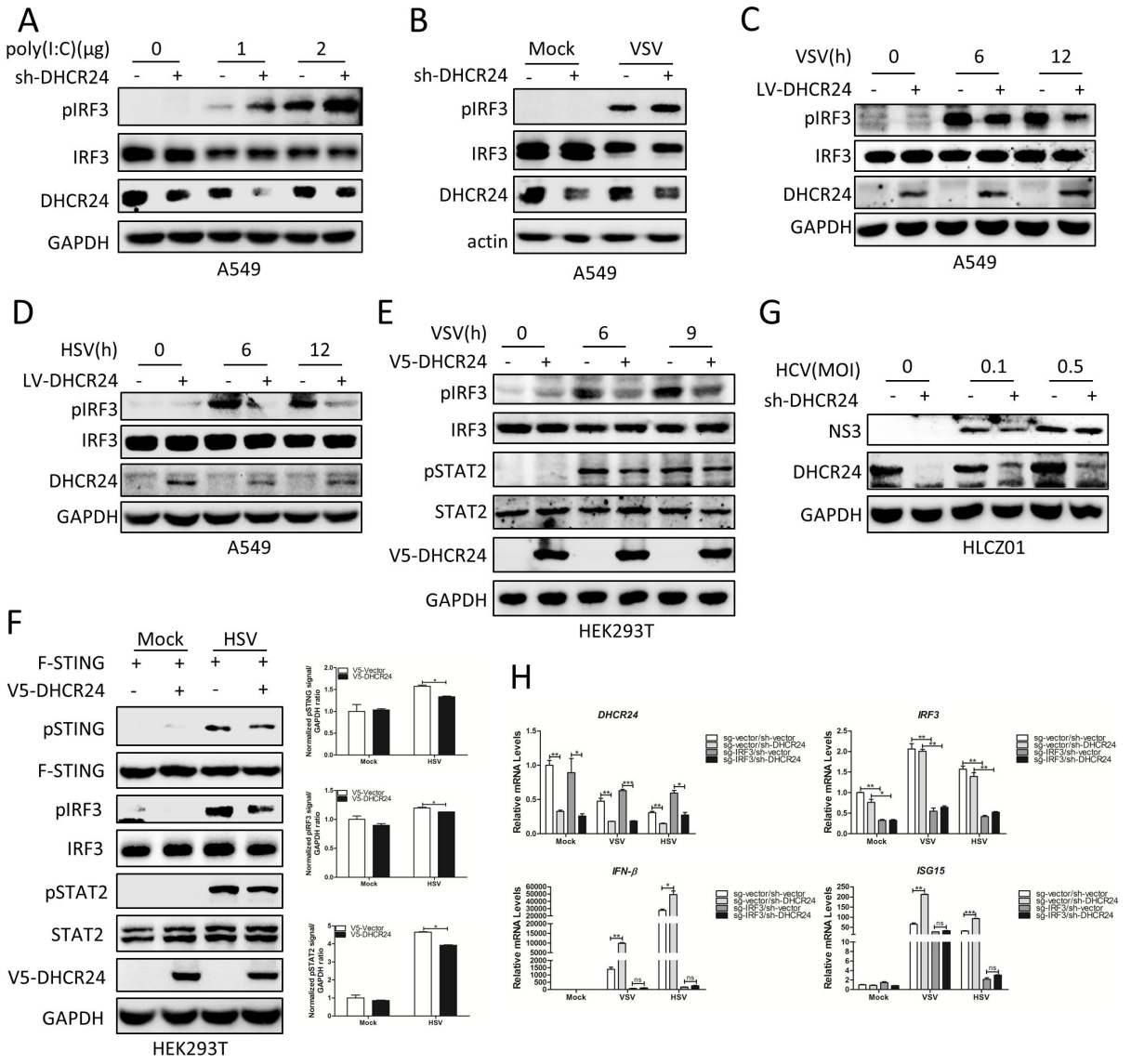

FIG 2 DHCR24 inhibits IRF3 activation triggered by RNA and DNA viruses. (A and B) Control cells or stable DHCR24-silenced A549 cells were transfected with 1.0 or 2.0 μg of HMW poly(I:C) for 12 h (A) or infected with VSV (MOI = 0.01) for 4 h (B) to check pIRF3, IRF3, DHCR24, GAPDH, and actin by immunoblotting assay. (C and D) A549 cells were treated with lentivirus-vector or lentivirus-DHCR24 for 48 h and then infected with VSV (MOI = 0.01) (C) or HSV (MOI = 0.01) (D) for the indicated times to check pIRF3, IRF3, DHCR24, and GAPDH by immunoblotting assay. (E and F) HEK293T cells transfected with pcDNA3.1a-V5-vector or pcDNA3.1a-V5-DHCR24 for 40 h and then infected with VSV (MOI = 0.05) (E) for the indicated times to check pIRF3, IRF3, pSTAT2, STAT2, V5-DHCR24, and GAPDH by immunoblotting assay or HSV (MOI = 0.05) for 9 h (F) to check pSTING, STING, pIRF3, IRF3, pSTAT2, STAT2, V5-DHCR24, and GAPDH by immunoblotting assay. (G) Control cells or stable DHCR24-silenced HLCZ01 cells were infected with HCV for 2 or 3 days to check NS3, DHCR24, and GAPDH by immunoblotting assay. (H) Wild-type or IRF3-knocked out A549 cells were treated with lentivirus-shvector or lentivirus-shDHCR24 for 72 h and then infected with VSV (MOI = 0.01) or HSV (MOI = 0.05) for 12 h. DHCR24, IRF3, IFN-β, and ISG15 mRNAs were measured by qRT-PCR and normalized with GAPDH. All experiments were repeated at least three times with consistent results. Bar graphs show the means "±" SD ($n = 3$). *$P < 0.05$, **$P < 0.01$, and ***$P < 0.001$.

was used (Fig. 3C). U18666A treatment augmented the expression of *IFN-β*, *IL-28A*, *IL-29*, *ISG15*, *IFITM1*, and *MX1* triggered by poly(I:C), RNA, or DNA viruses in human hepatocytes (Fig. 3D through F). Consistent with these results, IRF3 phosphorylation was enhanced in poly(I:C)-transfected Huh7 cells, NDV-infected Huh7 cells, VSV-infected HepG2 cells, and HSV-infected HLCZ01 cells treated with U18666A (Fig. 3G through J). Consistent with the enhanced IFN production, U18666A treatment inhibited VSV or HSV replication, as shown by the fluorescence of GFP-VSV or GFP-HSV in HLCZ01 cells (Fig. 3K and L).

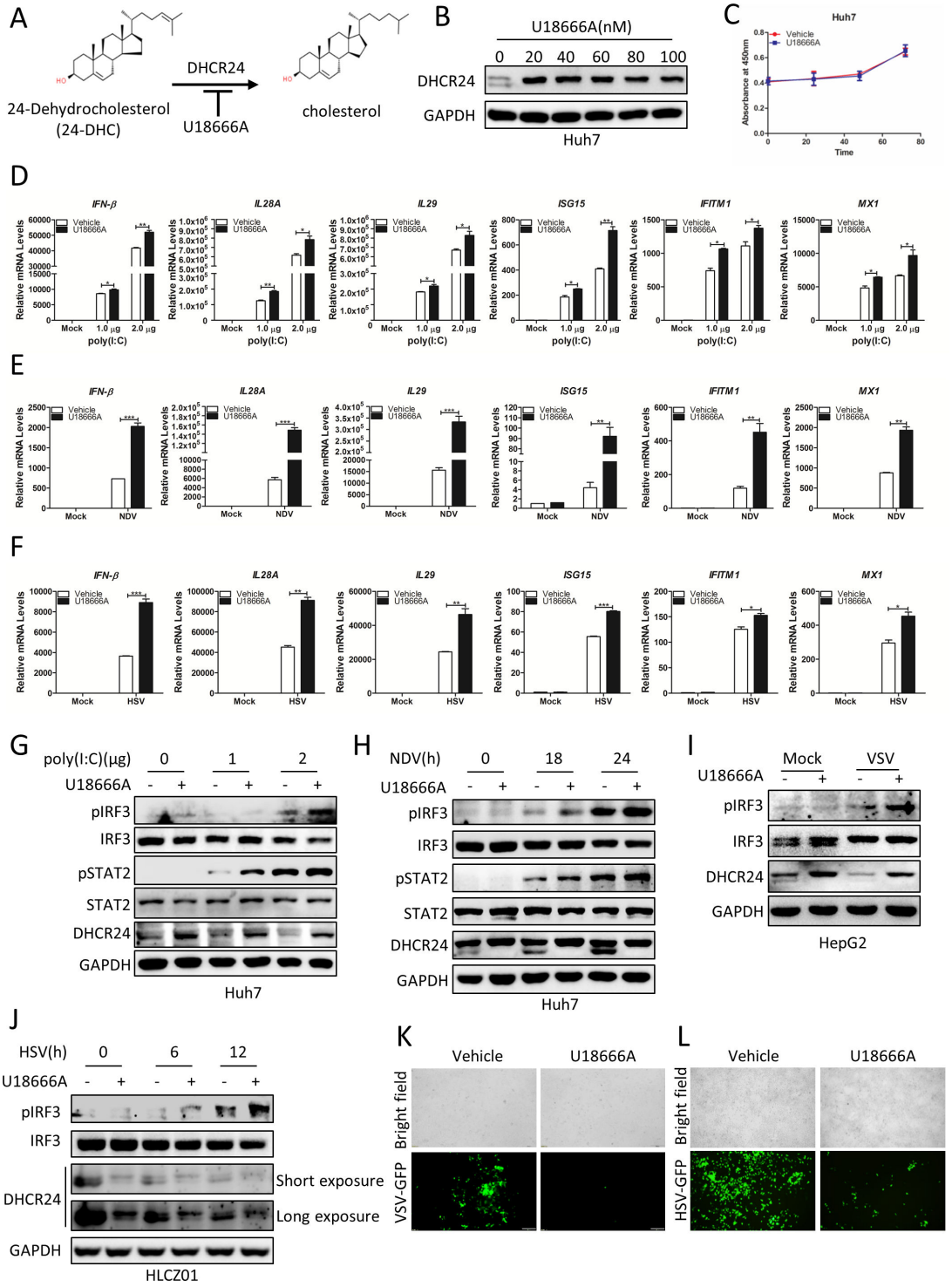

FIG 3 DHCR24 inhibitor U18666A positively regulates innate immune responses to multiple viral infections. (A) The diagram shows that DHCR24 converts 24-dehydrocholesterol (24-DHC) to cholesterol. (B) Huh7 cells were treated with the DHCR24 inhibitor U18666A 12 h for indicated doses to check DHCR24 and GAPDH by immunoblotting assay. (C) CCK-8 assays were used to determine the cell proliferation ability of U18666A-treated cells. (D–F) HLCZ01 cells were treated with U18666A (20 nM) for 12 h and then transfected with 1.0 μg or 2.0 μg of HMW poly(I:C) for 12 h (D) or infected with NDV (MOI = 0.01) for 36 h (E) and HSV (MOI = 0.5) for 12 h (F). IFN-β, IL-28A, IL-29, ISG15, IFITM1, and MX1 mRNAs were measured by qRT-PCR and normalized with GAPDH. (G) Huh7 cells were treated with U18666A (20 nM) for 12 h and then transfected with 1.0 or 2.0 μg of HMW poly(I:C) for 12 h to check pIRF3, IRF3, pSTAT2, STAT2, DHCR24, and GAPDH by immunoblotting assay. (H) Huh7 cells were treated with U18666A (20 nM) for 12 h and then infected with NDV (MOI = 0.05) for the indicated times to check pIRF3, IRF3, pSTAT2, STAT2, DHCR24, and GAPDH by immunoblotting assay. (I) HepG2 cells were treated with U18666A (20 nM) for 12 h and then infected with

(Continued on next page)

FIG 3 (Continued)

VSV (MOI = 1) for 12 h to check pIRF3, IRF3, DHCR24, and GAPDH by immunoblotting assay. (J) HLCZ01 cells were treated with U18666A (20 nM) for 12 h and then infected with HSV (MOI = 0.5) for the indicated times to check pIRF3, IRF3, DHCR24, and GAPDH by immunoblotting assay. (K and L) HLCZ01 cells were treated with U18666A (20 nM) for 12 h and then infected with VSV-GFP (MOI = 0.01) (K) or HSV-GFP (MOI = 0.02) (L) for 12 h to detect the amount of VSV–GFP or HSV–GFP by microscopy imaging. All experiments were repeated at least three times with similar results. Bar graphs show the means "±" SD (n = 3). *P < 0.05, **P < 0.01, and ***P < 0.001.

Since DHCR24 is the key enzyme that converts 24-DHC to cholesterol (Fig. 3A), DHCR24 decrease or inhibition may lead to 24-DHC accumulation and cholesterol reduction (19). We examined whether the increased 24-DHC plays a role in IFN-β production. As shown in Fig. 4A through C, 24-DHC increased *IFN-β*, *IL-28A*, and *MX1* mRNA production upon poly(I:C) transfection, and VSV or NDV infection in HLCZ01 cells, which was consistent with enhanced IRF3 phosphorylation (Fig. 4D and E). These data together suggest that the DHCR24 inhibitor U18666A positively regulates virus-triggered innate immune responses and can be used to defend against virus infection.

DHCR24 interacts with MAVS or STING

To determine the molecular mechanism of DHCR24 in RLR signaling, we performed coimmunoprecipitation (co-IP) assays to investigate the interaction between DHCR24 and various signaling molecules. DHCR24 was associated with MAVS, but not with any of the other examined components, including MDA5, RIG-I, TBK1, and IRF3 (Fig. 5A and B). The association between endogenous DHCR24 and MAVS was further confirmed by immunoprecipitation assays (Fig. 5C). To further determine which domain of MAVS interacts with DHCR24, we constructed a series of MAVS truncations. The data suggest that the transmembrane domain of MAVS is essential for the DHCR24-MAVS interaction (Fig. 5D and E). Moreover, the interaction between MAVS and DHCR24 was substantially decreased upon VSV infection (Fig. 5F). Because DHCR24 also negatively regulates DNA virus-induced signaling, we speculated that DHCR24 might target proteins involved in the DNA virus-triggered pathway. The co-IP experiments showed that DHCR24 precipitates with STING but not with cGAS (Fig. 5G and H). Furthermore, an association between endogenous DHCR24 and STING was confirmed in HLCZ01 cells (Fig. 5I). Domain mapping analysis suggested that the 161–220 section of STING is the key section for the STING-DHCR24 interaction (Fig. 5J and K). The interaction between STING and DHCR24 was weakened upon HSV infection (Fig. 5L). Together, these data demonstrate that DHCR24 interacts with MAVS or STING.

DHCR24 suppresses K27-linked ubiquitination and activation of MAVS

To investigate the underlying mechanism by which DHCR24 regulates MAVS function, we first examined the level of MAVS protein. DHCR24-silenced HLCZ01 cells were treated with cycloheximide (CHX), NH_4CL, or MG132. The level of MAVS protein remained unchanged after CHX treatment in DHCR24-silenced HLCZ01 cells (data not shown). Even after knockdown of DHCR24, neither NH_4CL nor MG132 treatment had any effects on the protein level of MAVS in HLCZ01 cells (data not shown), ruling out the possibility that DHCR24 affects the protein level of MAVS.

The activity and availability of MAVS are strictly regulated by ubiquitination (34–36). DHCR24 can competitively bind P53 with Mdm2, thus inhibiting P53 ubiquitination (26). Therefore, we tested whether DHCR24 regulates MAVS ubiquitination. As shown in Fig. 6A, ectopic expression of DHCR24 resulted in a progressive reduction in VSV-induced MAVS ubiquitination in a dose-dependent manner. Since different ubiquitin linkages are related to distinctive functions, we examined the type of ubiquitin linkage in MAVS that is inhibited by DHCR24. By transfecting K27-, K48-, or K63-specific linkage Ub mutants, we observed that DHCR24 inhibited the K27-linked, but not K48- or K63-linked, polyubiquitination of MAVS (Fig. 6B). Conversely, the K27-linked polyubiquitination of endogenous MAVS was increased in DHCR24 knockdown Huh7 cells (Fig. 6C). Our previous study

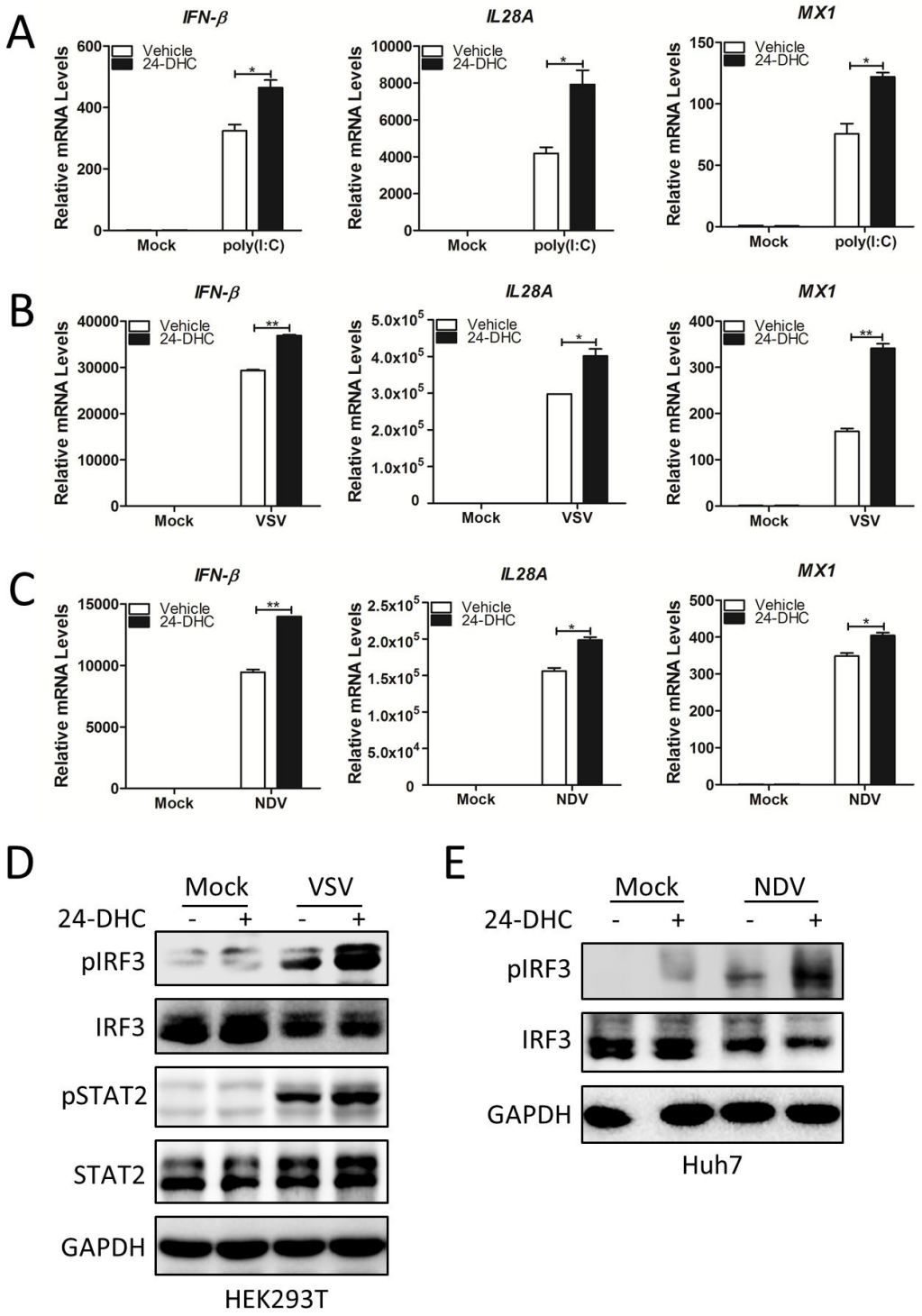

FIG 4 The natural cholesterol precursor 24-DHC promotes innate immune response to viral infection. (A–C) HLCZ01 cells pre-treated with 100 nM 24-DHC for 12 h and then transfected with 1.0 µg of HMW poly(I:C) for 12 h (A) or infected with VSV (MOI = 0.5) for 12 h (B) and NDV (MOI = 0.05) for 24 h (C). IFN-β, IL-28A, and MX1 mRNAs were measured by qRT-PCR and normalized with GAPDH. (D) HEK293T cells pre-treated with 100 nM 24-DHC for 12 h and then infected with VSV (MOI = 0.5) for 12 h to check pIRF3, IRF3, pSTAT2, STAT2, and GAPDH by immunoblotting assay. (E) Huh7 cells were treated with 100 nM 24-DHC for 12 h and then infected with NDV (MOI = 0.05) for 24 h to check pIRF3, IRF3, and GAPDH by immunoblotting assay. All experiments were repeated at least three times with consistent results. Bar graphs show the means "±" SD ($n = 3$). *$P < 0.05$, **$P < 0.01$, and ***$P < 0.001$.

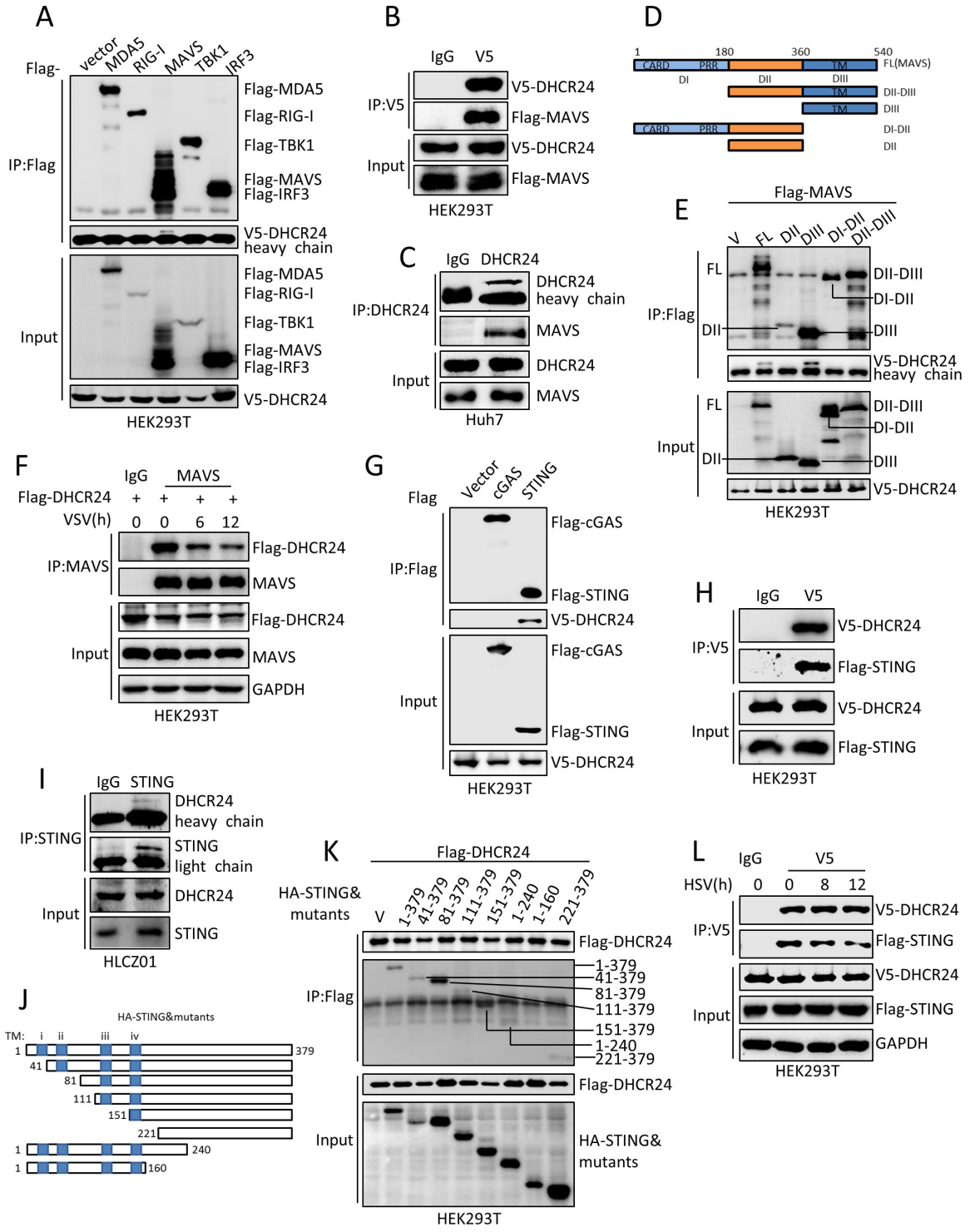

FIG 5 DHCR24 interacts with MAVS or STING. (A) HEK293T cells were transfected with the indicated plasmids for 48 h, and lysates were obtained. Immunoprecipitation and immunoblotting assays were performed with the indicated antibodies. (B) HEK293T cells were transfected with p3×Flag MAVS and pcDNA3.1a-V5-DHCR24 for 48 h. The lysates were immunoprecipitated with control IgG or anti-V5 antibody, and immunoblotting assays were performed with anti-Flag or anti-V5 antibody. (C) Lysates of Huh7 cells were immunoprecipitated with control IgG or anti-DHCR24 antibody, and immunoblotting assays were performed with anti-DHCR24 or anti-MAVS antibody. (D) A schematic presentation of full-length MAVS and MAVS truncations. (E) HEK293T cells were transfected with the indicated plasmids for 48 h. Lysates were immunoprecipitated with anti-Flag antibody. Immunoblotting assays were performed with anti-V5 or anti-Flag antibody. (F) HEK293T cells were transfected with p3×Flag-DHCR24 for 36 h and then infected with VSV (MOI = 0.05) for the indicated times. Lysates were immunoprecipitated with anti-MAVS, and immunoblotting assays were performed with indicated antibodies. (G) HEK293T cells were transfected with the (Continued on next page)

FIG 5 (Continued)

plasmids pcDNA3.1a-V5-DHCR24 and p3×Flag-vector, p3×Flag cGAS, or p3×Flag-STING for 48 h. Lysates were immunoprecipitated with anti-V5 antibody, and immunoblotting assays were performed with anti-V5 or anti-Flag antibody. (H) HEK293T cells were transfected with p3×Flag-STING and pcDNA3.1a-V5-DHCR24 for 48 h. The lysates were immunoprecipitated with control IgG or anti-V5 antibody, and immunoblotting assays were performed with anti-Flag or anti-V5 antibody. (I) Lysates of HLCZ01 cells were immunoprecipitated with control IgG or anti-STING antibody, and immunoblotting assays were performed with anti-DHCR24 or anti-STING antibody. (J) A schematic presentation of full-length STING and STING truncations. (K) HEK293T cells were transfected with the indicated plasmids for 48 h. Lysates were immunoprecipitated with anti-Flag antibody, and immunoblotting assays were performed with anti-HA or anti-Flag antibody. (L) HEK293T cells were transfected with p3×Flag-STING and pcDNA3.1a-V5-DHCR24 for 36 h and then infected with HSV (MOI = 0.05) for the indicated times. Lysates were immunoprecipitated with anti-V5, and immunoblotting assays were performed with indicated antibodies. All experiments were repeated at least three times with similar results.

showed that the E3 ubiquitin ligase TRIM21 promotes K27-linked ubiquitination of MAVS (37). We hypothesized that DHCR24 might regulate TRIM21-mediated MAVS ubiquitination. We first examined whether there was a relationship between DHCR24 and TRIM21. Both exogenous and endogenous co-IP showed that there was a strong interaction between DHCR24 and TRIM21 (Fig. 6D and E). Moreover, DHCR24 potently inhibited TRIM21-induced K27-linked ubiquitination of MAVS (Fig. 6F). Consistently, DHCR24 blocked the recruitment of TBK1 to MAVS and suppressed downstream signaling (Fig. 6G). Then, we determined whether DHCR24 enzyme activity is required for its function in regulating MAVS ubiquitination. The results from the Western blotting assay showed that the inhibitory effect of DHCR24 on TRIM21-induced MAVS ubiquitination was reversed after the addition of U18666A (Fig. 6H). The K27-linked polyubiquitination of endogenous MAVS was increased in U18666A-treated Huh7 cells (Fig. 6I). We also wanted to know how the interaction between DHCR24, MAVS, and TRIM21 maintains the balance. We transfected pFlag-tagged TRIM21 and pV5-tagged DHCR24 into HEK293T cells, followed by co-IP assays. However, the gradual increase in DHCR24 had no effect on the interaction between MAVS and TRIM21 (Fig. 6J). Importantly, knocking down MAVS abolished the induction of IFNs by NDV infection in DHCR24-silenced cells (Fig. 6K). Finally, to consolidate that DHCR24 inhibits TRIM21-mediated MAVS ubiquitination, we checked IFN induction in TRIM21-silenced cells following DHCR24 silence. Consistently, knocking down TRIM21 abolished the induction of IFNs by VSV infection in DHCR24-silenced cells (Fig. 6L). Overall, these findings supported that DHCR24 inhibits K27-linked ubiquitination and activation of MAVS for the negative regulation of RLR signaling.

DHCR24 inhibits K27-linked ubiquitination and activation of STING

Our data showed that DHCR24 negatively regulates the innate immune responses induced by both RNA and DNA viruses, and DHCR24 also interacts with STING. We speculated that DHCR24 may regulate STING function in the same manner. As expected, enforced expression of DHCR24 markedly inhibited the ubiquitination of STING (Fig. 7A). To examine the type of DHCR24-mediated ubiquitin linkage of STING, we transfected wild-type ubiquitin or ubiquitin mutants that retain a single lysine residue (KO) in the presence or absence of DHCR24. Further ubiquitination assay results showed that the overexpression of DHCR24 diminished K27O ubiquitin conjugation to STING (Fig. 7B). It has been reported that AMFR catalyzes K27-linked ubiquitination of STING (38). To explore the relationship among DHCR24, STING, and AMFR, we first analyzed the connection between DHCR24 and AMFR. Surprisingly, there was a strong interaction between DHCR24 and AMFR (Fig. 7C and D). In HEK293T cells, Flag-tagged STING was cotransfected with pcDNA3.1a-3×Flag AMFR, V5-tagged DHCR24, and HA-tagged K27O ubiquitin. Consistent with the literature report (38), the overexpression of AMFR profoundly promoted K27-linked ubiquitination of STING, but this phenomenon was weakened in the presence of DHCR24 (Fig. 7E). K27-linked ubiquitination of STING is critical for its recruitment of TBK1. We examined whether DHCR24 affects the association between STING and TBK1. Consistently, the overexpression of DHCR24 inhibited STING-TBK1 interaction in a dose-dependent manner (Fig. 7F). Next, we also tested the effect of the DHCR24 inhibitor U18666A on STING ubiquitination. Western blotting assays showed

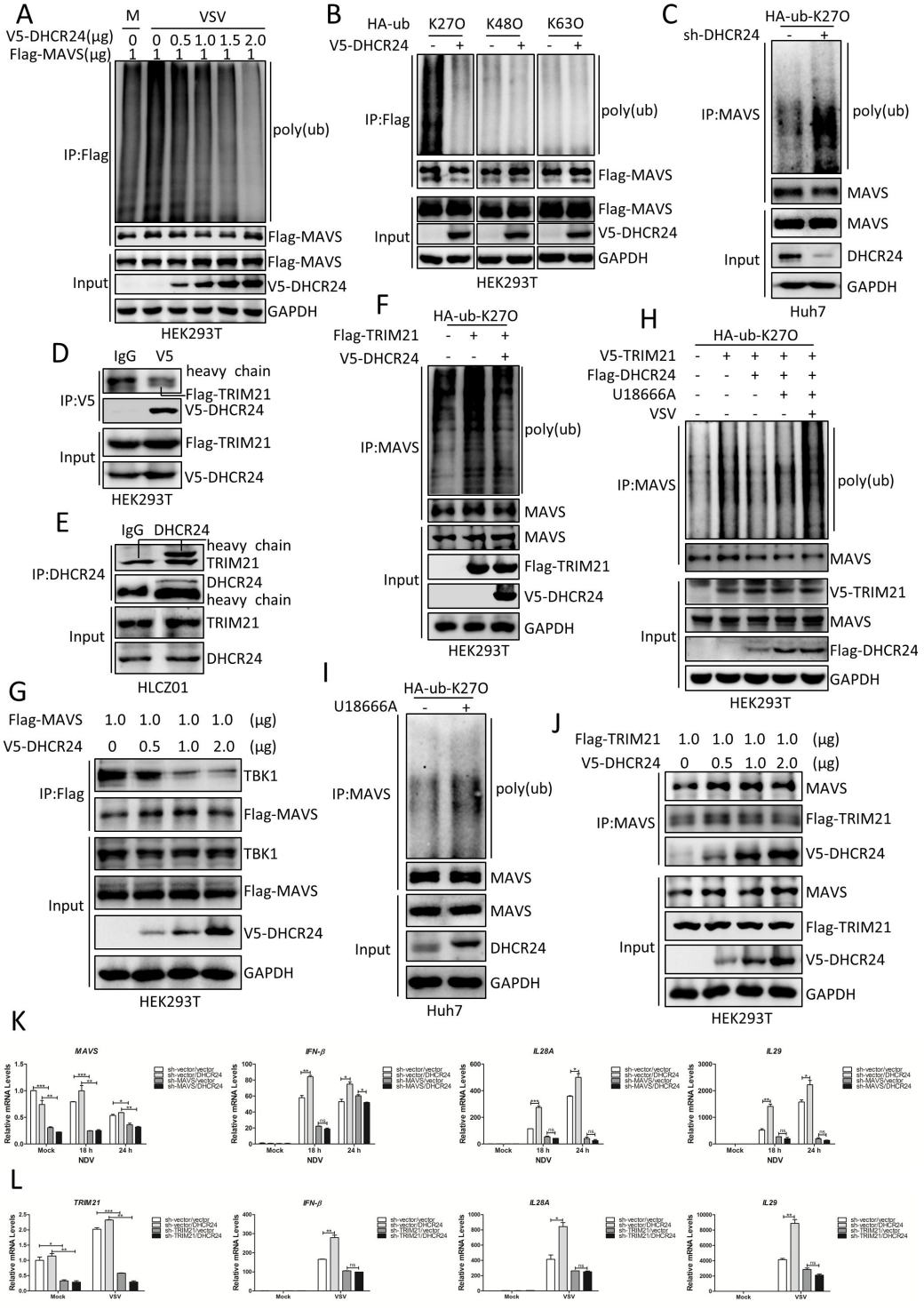

FIG 6 DHCR24 inhibits K27-linked ubiquitination of MAVS. (A) HEK293T cells were transfected with the indicated plasmids for 42 h, then treated with VSV (MOI = 0.05) and MG132 (25 μM) for additional 6 h. Ubiquitination and immunoblotting assays were performed with indicated antibodies. (B) HEK293T cells were cotransfected with K27O-, K48O-, or K63O-linked HA-ub plasmid with p3×Flag MAVS and pcDNA3.1a-V5-DHCR24 for 42 h and then treated with MG132 (25 μM) for additional 6 h. Ubiquitination and immunoblotting assays were performed with indicated antibodies. (C) Control cells or stable DHCR24-silenced Huh7 cells were transfected with K27O-linked HA-ub for 42 h and then treated with MG132 (25 μM) for additional 6 h. Ubiquitination and immunoblotting assays were performed with indicated antibodies. (D) HEK293T cells were transfected with p3×Flag-TRIM21 and pcDNA3.1a-V5-DHCR24 for 48 h. The lysates were immunoprecipitated with anti-V5 antibody, and (Continued on next page)

FIG 6 (Continued)

immunoblotting assays were performed with anti-V5 or anti-Flag antibody. (E) Lysates of HLCZ01 cells were immunoprecipitated with control IgG or anti-DHCR24 antibody, and immunoblotting assays were performed with anti-DHCR24 or anti-TRIM21 antibody. (F) HEK293T cells were transfected with K27O-linked HA-ub, p3×Flag-TRIM21, and pcDNA3.1a-V5-DHCR24 for 42 h and then treated with MG132 (25 μM) for additional 6 h. Ubiquitination and immunoblotting assays were performed with indicated antibodies. (G) HEK293T cells were transfected with p3×Flag MAVS and an increased amount of DHCR24 expression plasmid for 48 h. The lysates were performed with immunoprecipitation and immunoblotting assays with the indicated antibodies. (H) HEK293T cells were transfected with K27O-linked HA-ub, p3×Flag-DHCR24 and pcDNA3.1a-V5-TRIM21 for 36 h, then added U18666A (20 nM) for 6 h, treated with VSV (MOI = 0.05) and MG132 (25 μM) for additional 6 h. Ubiquitination and immunoblotting assays were performed with indicated antibodies. (I) Huh7 cells were transfected with K27O-linked HA-ub for 36 h, then added U18666A (20 nM) for 6 h, treated with MG132 (25 μM) for additional 6 h. Ubiquitination and immunoblotting assays were performed with indicated antibodies. (J) HEK293T cells were transfected with p3×Flag-TRIM21 and an increased amount of DHCR24 expression plasmid for 48 h. The lysates were obtained, and immunoprecipitation and immunoblotting assays were performed with the indicated antibodies. (K) Control cells or stable DHCR24-silenced Huh7 cells were infected with lentivirus-shMAVS for 48 h and then infected with NDV (MOI = 0.001) for the indicated times. MAVS, IFN-β, IL-28A, and IL-29 mRNAs were measured by qRT-PCR and normalized with GAPDH. (L) Control cells or stable DHCR24-silenced Huh7 cells were infected with lentivirus-shTRIM21 for 48 h and then infected with VSV (MOI = 0.5) for 9 h. TRIM21, IFN-β, IL-28A, and IL-29 mRNAs were measured by qRT-PCR and normalized with GAPDH. All experiments were repeated at least three times with consistent results. Bar graphs show the means "±" SD ($n = 3$). *$P < 0.05$, **$P < 0.01$, and ***$P < 0.001$.

that K27-linked ubiquitination of STING was strongly inhibited in the presence of DHCR24, but this phenomenon was reversed after the addition of U18666A (Fig. 7G). Consistently, K27-linked ubiquitination of endogenous STING was increased in U18666A-treated HLCZ01 cells (Fig. 7H). We also examined the interactions between DHCR24, STING, and AMFR. However, the gradual increase in DHCR24 had no effect on the interaction between STING and AMFR (Fig. 7I). Finally, we wondered whether the impact of DHCR24 is specific to innate immunity-related K27-ubiquitination targets. Therefore, we chose BRAF, a protein that can undergo K27-linked ubiquitination but unrelated to innate immune signaling pathways, to examine the effect of DHCR24 on K27-linked ubiquitination. Unexpectedly, using the two-step immunoprecipitation assay, DHCR24 did affect the K27-linked ubiquitination of BRAF (Fig. 7J), this suggests that DHCR24 may regulate global K27-ubiquitination, but more experimental data are needed to prove this. Taken together, these data demonstrate that DHCR24 inhibits the recruitment of TBK1 to STING by impacting AMFR catalyzes the K27-linked ubiquitination on STING.

U18666A protects mice from virus infection *in vivo*

Studies have shown that DHCR24$^{-/-}$ mice die within a few hours after birth (39). Therefore, we used the DHCR24 inhibitor U18666A to examine whether it protects mice from viral infection. Mice were treated daily with U18666A for 3 days, followed by VSV infection (Fig. 8A). We measured the cholesterol level in the sera of the mice. U18666A treatment profoundly reduced cholesterol and increased IFN-β protein levels in the serum in VSV- or HSV-infected mice (Fig. 8B through 8D). Consistently, the expression of *Ifnb* in the lung, liver, spleen, and kidney was significantly increased in U18666A-treated mice compared to the control mice upon virus infection (Fig. 8E and F). The level of VSV mRNA and the viral load of VSV and HSV in the liver decreased after U18666A treatment (Fig. 8G and H). Consistently, the U18666A-treated mice had improved survival rates following VSV and HSV infection (Fig. 8I and J). All the data suggest that the loss of DHCR24 protects mice from viral infection by enhancing the induction of IFNs.

DISCUSSION

Lipid metabolism is crucial to many physiological processes (40, 41). In particular, cholesterol metabolism-related proteins and products play an important role in the regulation of innate immunity. For example, CH25H is a broad antiviral ISG (3). Targeting

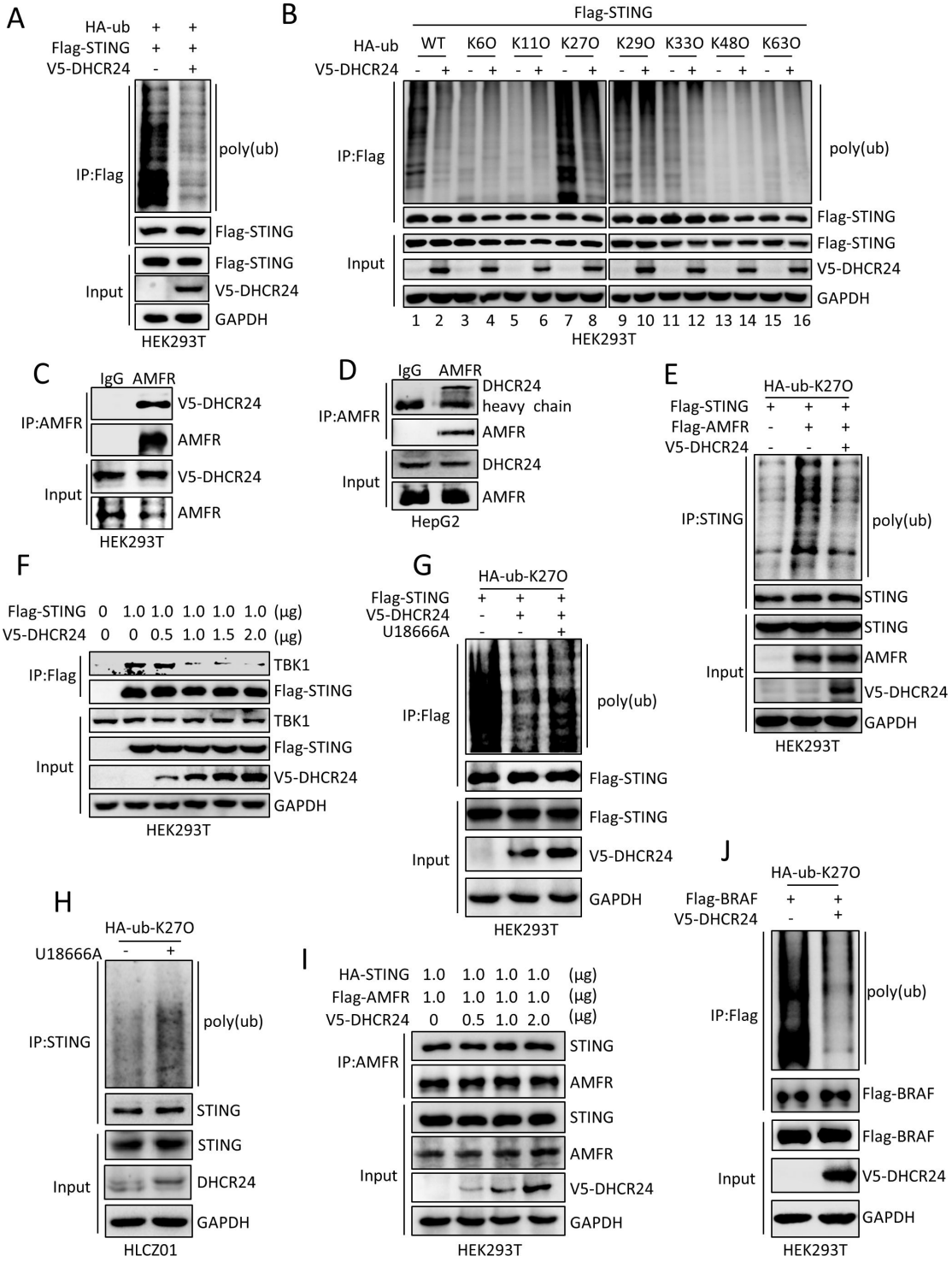

FIG 7 DHCR24 inhibits K27-linked ubiquitination of STING. (A) HEK293T cells were transfected with HA-ub, p3×Flag-STING, and pcDNA3.1a-V5-DHCR24 for 42 h and then treated with MG132 (25 μM) for additional 6 h. Lysates were obtained, and ubiquitination and immunoblotting assays were performed with indicated antibodies. (B) HEK293T cells were transfected with wild type (WT) or K6O-, K11O-, K27O-, K33O-, K48O-, or K63O-linked HA-ub plasmid, p3×Flag-STING, and pcDNA3.1a-V5-DHCR24 for 42 h and treated with MG132 (25 μM) for additional 6 h. Lysates were obtained, and ubiquitination and immunoblotting assays were performed with indicated antibodies. (C) HEK293T cells were transfected with the pcDNA3.1a-3×Flag AMFR and pcDNA3.1a-V5-DHCR24 plasmids for 48 h. Lysates were immunoprecipitated with anti-AMFR antibody, and immunoblotting assays were performed with anti-V5 or anti-AMFR antibody. (D) Lysates of HepG2 cells were immunoprecipitated with control IgG or anti-AMFR antibody, and immunoblotting assays were performed with anti-DHCR24 or anti-AMFR antibody. (E) HEK293T cells were transfected with K27O-linked HA-ub, pcDNA3.1a-3×Flag AMFR, p3×Flag-STING, and pcDNA3.1a-V5-DHCR24 for 42 h and (Continued on next page)

FIG 7 (Continued)

treated with MG132 (25 μM) for additional 6 h. Lysates were obtained, and ubiquitination and immunoblotting assays were performed with indicated antibodies. (F) HEK293T cells were transfected with p3×Flag-STING and an increased amount of DHCR24 expression plasmids for 48 h. Lysates were obtained, and ubiquitination and immunoblotting assays were performed with the indicated antibodies. (G) HEK293T cells were transfected with K27O-linked HA-ub, p3×Flag-STING, and pcDNA3.1a-V5-DHCR24 for 36 h, added U18666A (20 nM) for 6 h, then treated with MG132 (25 μM) for additional 6 h. Lysates were obtained, and ubiquitination and immunoblotting assays were performed with indicated antibodies. (H) HLCZ01 cells were transfected with K27O-linked HA-ub plasmid for 36 h, added U18666A (20 nM) for 6 h, then treated with MG132 (25 μM) for additional 6 h. Lysates were obtained, and ubiquitination and immunoblotting assays were performed with indicated antibodies. (I) HEK293T cells were transfected with HA-STING, pcDNA3.1a-3×Flag AMFR, and an increased amount of DHCR24 expression plasmid for 48 h. The lysates were obtained, and immunoprecipitation and immunoblotting assays were performed with the indicated antibodies. (J) HEK293T cells were transfected with K27O-linked HA-ub plasmid, p3×Flag BRAF, and pcDNA3.1a-V5-DHCR24 for 42 h and treated with MG132 (25 μM) for additional 6 h. Lysates were obtained, and ubiquitination and immunoblotting assays were performed with indicated antibodies. All experiments were repeated at least three times with consistent results.

DHCR7 enhances IRF3 phosphorylation and IFN-I production (5). In this study, we found that DHCR24, a key enzyme that catalyzes 24-DHC to cholesterol, is downregulated in pathogen-infected hepatocytes, and DHCR24 plays a negative regulatory role in innate immunity (Fig. 9).

In our study, several lines of evidence substantiate the role of DHCR24 in innate antiviral signaling. First, the deficiency of endogenous DHCR24 promotes virus-induced IFN and ISG production, consistent with decreased viral replication. Second, U18666A, an inhibitor of DHCR24 activity, augments IRF3 phosphorylation and IFN production upon RNA or DNA viral infection. Since we observed that U18666A has a strong antiviral capacity, we speculate that in addition to its inhibiting effect on DHCR24, U18666A may also act on VSV and HSV itself as it does on the dengue virus itself. Third, DHCR24 knockdown or inhibition reduces cholesterol and increases 24-DHC. Here, we found that 24-DHC-treated hepatocytes express more IFNs and ISGs when challenged with a virus. Therefore, 24-DHC may be a potential drug against a variety of viruses. However, the mechanisms of how 24-DHC enhances innate immunity need to be further investigated. Fourth, DHCR24 targets two key proteins, MAVS and STING, and inhibits their functions. Fifth, the DHCR24 inhibitor U18666A protects mice from RNA and DNA viral infections.

MAVS and STING are the key adapter proteins of RLR signaling and cGAS-STING signaling, respectively. The functions of MAVS and STING are strictly controlled to achieve signal balance, including ubiquitination and deubiquitinaion. It has been previously shown that the E3 ligase TRIM31 exerts K63 linkage specificity to MAVS and positively regulates the activity of MAVS (35). The deubiquitinase OTUD3 directly hydrolyzes K63-linked polyubiquitination of MAVS, negatively regulating the activity of MAVS (42). In the current study, we confirmed that TRIM21 promoted K27-linked polyubiquitination of MAVS, which is consistent with our previous study (37). Further study revealed that DHCR24 directly interacts with MAVS and TRIM21, specifically decreasing the TRIM21-dependent K27-linked polyubiquitination of MAVS, thus restraining the recruitment of TBK1 to MAVS and inhibiting innate immune responses.

In addition to suppressing K27-linked polyubiquitination of MAVS, DHCR24 represses K27-linked polyubiquitination of STING, which impairs the recruitment of TBK1 to STING as well as cellular responses against DNA viral infection. Previous studies suggest that the E3 ligase RNF115 induces K63-linked ubiquitination of STING after HSV infection, which promotes the aggregation of STING and subsequent recruitment of TBK1 (43). USP13 deconjugates K27-linked polyubiquitin chains from STING and thereby inhibits the recruitment of TBK1 to turn down antiviral immune responses (44). AMFR constitutively interacts with and mediates K27-linked ubiquitination of STING (38). Our results show the regulatory effect of AMFR on STING and demonstrate that the basal ubiquitination of STING mediated by AMFR and the interaction between TBK1 and STING are decreased in DHCR24 overexpressing cells. Moreover, to explore whether DHCR24 regulates K27-ubiquitination globally or specifically targeting RNA/DNA sensing signaling, we tested whether K27-linked ubiquitination of BRAF, which is unrelated to MAVS or STING, was altered by DHCR24. Unexpectedly, the ubiquitination assay showed that DHCR24 does

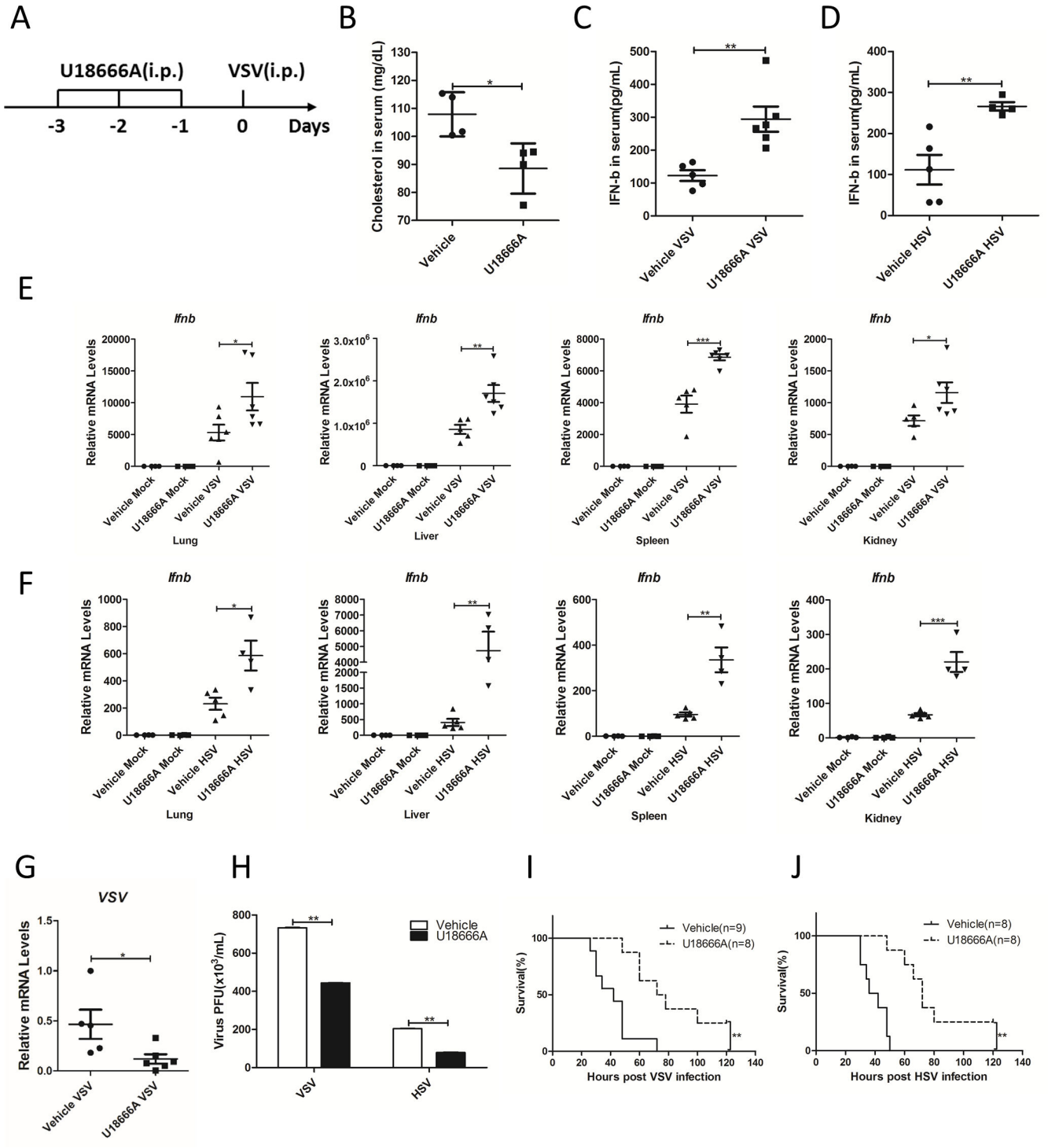

FIG 8 U18666A renders the mice resistance to various viral infection. (A) A scheme of U18666A treatment and viral infection of mice. (B) Serum cholesterol was detected after U18666A treatment for 3 days before VSV infection. (C) Serum IFN-β concentrations were detected by ELISA after the VSV (1×10^7 PFU/g, i.p.) infection for 24 h. (D) Serum IFN-β concentrations were detected by ELISA after the HSV (1×10^7 PFU/g, i.p.) infection for 18 h. (E and F) WT mice pre-treated with U18666A were infected with VSV (1×10^7 PFU/g, i.p.) for 24 h (E) or HSV (1×10^7 PFU/g, i.p.) for 18 h (F), and IFN-β mRNAs were measured by qRT-PCR and normalized with GAPDH. (G) WT mice pre-treated with U18666A were infected with VSV (1×10^7 PFU/g, i.p.) for 24 h, and liver VSV mRNAs were measured by qRT-PCR and normalized with GAPDH. (H) WT mice pre-treated with U18666A were infected with VSV (1×10^7 PFU/g, i.p.) for 24 h (E) or HSV (1×10^7 PFU/g, i.p.) for 18 h, and the liver VSV and HSV PFU were checked by plaque assay. (I and J) WT mice pre-treated with U18666A were infected with VSV (1×10^7 PFU/g, i.p.) (I) or HSV (1×10^7 PFU/g, i.p.) (J) to examine the survival rates. All experiments were repeated at least three times with similar results. Bar graphs show the means "±" SD ($n = 3$). *$P < 0.05$, **$P < 0.01$, and ***$P < 0.001$.

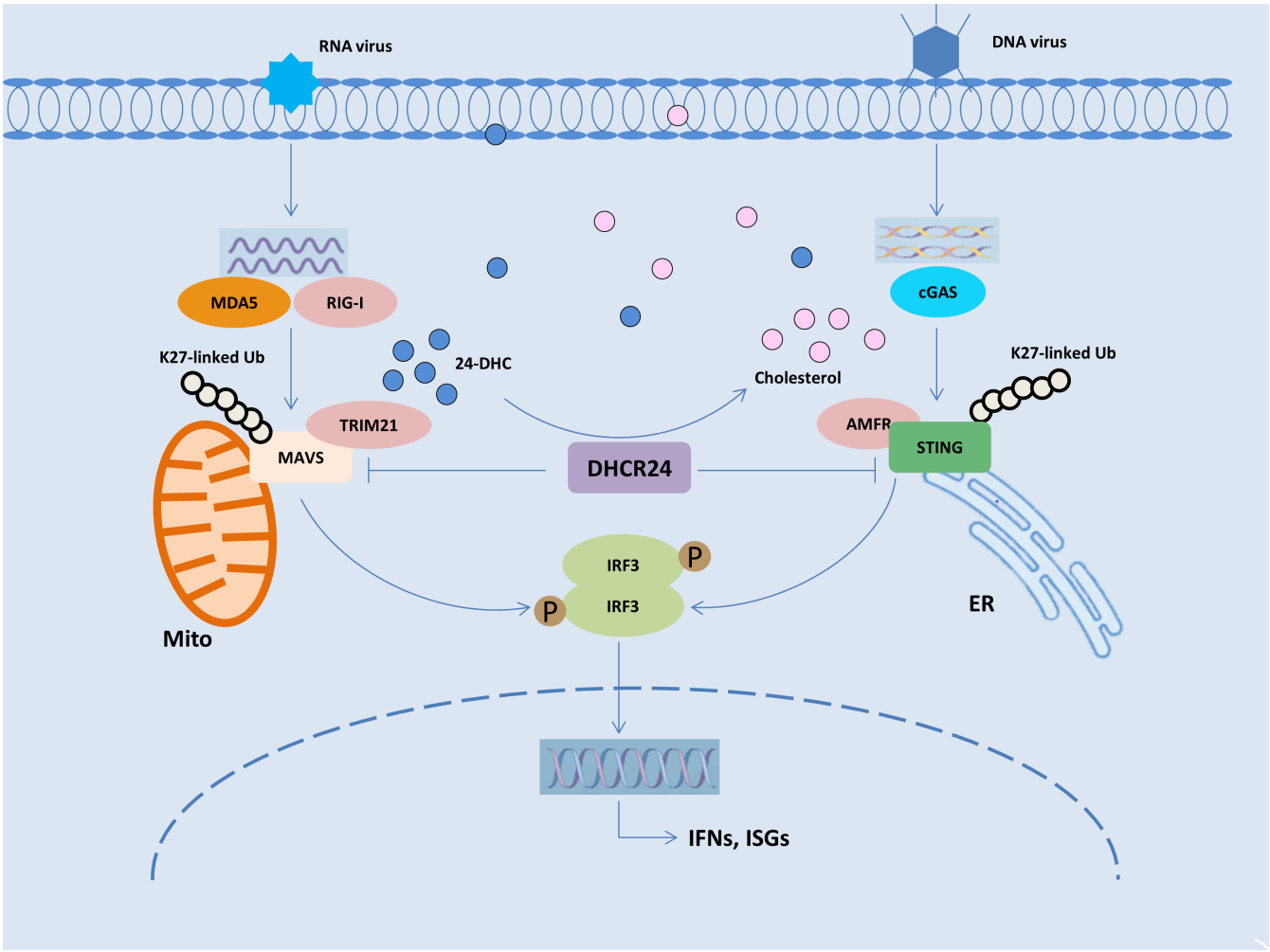

FIG 9 Mechanism diagram of DHCR24 regulating innate immune responses to viral infection. On the one hand, DHCR24 interacts with MAVS and impairs K27-linked polyubiquitination of MAVS mediated by TRIM21, inhibiting the recruitment of TBK1 to restrict innate immune response to RNA viral infection. On the other hand, DHCR24 interacts with STING and represses K27-linked polyubiquitination of STING by AMFR, blocking the recruitment of TBK1 and subsequently inhibiting innate immune response to DNA viral infection.

affect the K27-linked ubiquitination of BRAF. This is an interesting phenomenon and suggests that DHCR24 may regulate global K27-ubiquitination, but more experimental results are needed to clarify the mechanism and significance of this regulatory role of DHCR24 under different physiological signals.

We reveal for the first time that DHCR24 plays a critical role in innate immunity, in addition to promoting the innate immune response by using compound U18666A, which inhibits DHCR24 enzyme activity and increases metabolite of the 24-DHC. DHCR24 can directly interact with MAVS or STING and inhibit the ubiquitination of both proteins, thus inhibiting their activation. However, how the enzyme activity of DHCR24 affects the ubiquitination of MAVS and STING remains unclear at this time. We considered the possibility that inhibition of DHCR24 enzyme activity led to reduced cholesterol production, thereby promoting the ubiquitination activation of MAVS and STING. Whether DHCR24 has other lipid modifications, such as palmitoylation and geranyl acylation, on MAVS, STING, or other signaling proteins, is worth exploring. Another unresolved issue is why viral infection inhibits the expression of DHCR24. Sterols, hormones, growth factors, and epigenetics can affect the regulation of DHCR24. Studies have supported a link between SREBP activity and DHCR24 expression (45, 46). We

also prefer the hypothesis that virus infection regulates DHCR24 expression by affecting SREBP activity.

In summary, our findings elucidate a novel mechanism by which DHCR24 controls antiviral innate immune response and provides a basis for improving immunity by targeting DHCR24 functions.

MATERIALS AND METHODS

Mice

Mice with a C57BL/6 background were purchased from Hunan SJA Laboratory Animal Company. All mice were housed in a specific pathogen-free animal facility at Hunan University and randomly allocated to experimental groups with the same age (7–8 weeks) and sex (male). All animal experiments were performed under protocols approved by the Institutional Animal Care and Use Committee of Hunan University.

U18666A treatment and viral infection

Inhibitor U18666A (TargetMol, USA) was injected intraperitoneally into C57BL/6 WT mice at a dose of 10 mg/kg at the appointed time and then infected intraperitoneally with VSV or HSV (1×10^7 PFU/g). Blood was collected from the orbital sinus of the mice for cholesterol detection, and lung, liver, spleen, and kidney tissues were obtained from each mouse for analysis of RNA and viral titers at the indicated time points.

Cells

HLCZ01 cells were established in our laboratory in 2014. Huh7, HepG2, A549, and HEK293T cells were purchased from ATCC. HLCZ01 cells were cultured in collagen-coated tissue culture plates containing Dulbecco's modified Eagle medium (DMEM)-F-12 medium supplemented with 10% (vol/vol) fetal bovine serum (FBS; Gibco), 40 ng/mL of dexamethasone (Sigma), insulin-transferrin-selenium (ITS; Lonza), penicillin, and streptomycin. Other cells were propagated in DMEM supplemented with 10% FBS, L-glutamine, nonessential amino acids, penicillin, and streptomycin.

Antibodies and reagents

Antibodies included anti-DHCR24 (Santa Cruz, sc-390037, 1:100), anti-pIRF3 (CST, 4947S, 1:1000), anti-IRF3 (CST, 4302S, 1:1000), anti-pSTING (CST, 50907S, 1:1000), anti-STING (CST, 13647S, 1:1000), anti-pSTAT2 (CST, 88410S, 1:1000), anti-STAT2 (CST, 72604S, 1:1000), anti-TBK1 (CST, 38066S, 1:1000), anti-MAVS (Santa Cruz, sc-166583, 1:1000 and CST, 24930S, 1:1000), anti-TRIM21 (ABCAM, AB285367, 1:1000), anti-AMFR (Proteintech, 16675–1-AP, 1:1000), anti-GAPDH (Millipore, MAB374, 1:5000), anti-actin (Sigma, A5441-1, 1:5000), anti-Flag (Sigma, F3165, 1:5000), anti-V5 (Invitrogen, R960-25, 1:5000), and anti-HA (Abcam, ab236632, 1:5000). Reagents included DMSO (Sigma, D2650), MG132 (APExBIO Technology, C3348), puromycin (Thermo, A1113803), poly(I:C) HMW (Invivogen, tlrl-pic), and 24-dehydrocholesterol (Avanti, 700060P).

shRNA and sgRNA

shRNA targeting DHCR24-, MAVS-, and TRIM21 was cloned and inserted into the pGreenPuro shRNA expression lentivector plasmid. The sequence 5′-GCTGAATAGCATT GGCAATTA-3′ was targeted for human DHCR24. The sequence 5′-ATGTGGATGTTGTAGAG ATTC-3′ was targeted for human MAVS. The sequence 5′-GGCATGGTCTCCTTCTACAAC-3′ was targeted for human TRIM21. The sgRNA targeting IRF3 was cloned and inserted into the plentiCRISPRv2 plasmid. The sequence 5′-GCCAACCTGGAAGAGGAAT-3′ was targeted for human IRF3.

Plasmid construction

DHCR24 cDNA was synthesized from the total cellular RNA isolated from HLCZ01 cells by standard reverse transcription-PCR (RT-PCR). Subsequently, it was cloned and inserted into the pcDNA3.1a-V5-vector, p3×Flag CMV vector, or pCDH-CMV-MCS-EF1 lentivector by standard molecular biology techniques. The primers for amplifying DHCR24 were forward primer 5′-GGAATTCCGGCGCCGCACCATGGAGCCCGCCGTG-3′ and reverse primer 5′- GCTCTAGAGTGCCTGGCGGCCTTGCAGA-3′. IFN-β and ISRE luciferase reporter plasmids- and mammalian expression plasmids for Flag-MAVS and its mutants, ubiquitin, and its mutants, MDA5, RIG-I, TBK1, IRF3, and TRIM21, were described in our previous study (42). Flag-cGAS, Flag- and HA-STING, and their mutants were kindly provided by Hongbing Shu (Wuhan University, Wuhan, China). pcDNA3.1a-3×Flag AMFR was kindly provided by Yang Xiao (Central South University, Changsha, China). pEnCMV-BRAF-3×Flag (P11882) was obtained from MiaoLingBio, China.

Lentivirus production and generation of stable knockdown cell lines

In total, 8 µg target plasmid encoding shRNA or plentiCRISPRv2 encoding sgRNA, along with 8 µg lentivirus packaging plasmids psPAX2 and 2.7 µg envelope plasmid pMD2.G, were cotransfected into HEK293T cells using polyethylenimines (Polysciences). After 24 h, the culture medium was replaced with fresh medium. The viruses in the conditioned medium were harvested every 12 h, filtered with 0.45 µm filters (Millex) and stored at −80 °C. HLCZ01, A549, or Huh7 cells were plated in six-well plates and infected with the lentivirus for 72 h. The lentivirus-infected cells were selected for at least 7 days using puromycin (2 mg/mL) and subjected to the required assays.

Generation of CRISPR-Cas9-mediated stable knockout cell lines

Cells were plated in six-well plates prior to being transduced with 500 µL/well lentivirus produced with plentiCRISPRv2 in HEK293T cells. 72 h later, the cells were digested by trypsin, transferred into 96-well plates, and subjected to selection with puromycin (2 mg/mL). The single-cell clones were selected and identified by western blotting.

Viruses

VSV and HSV-1 were propagated and amplified in HEK293T cells. NDV was propagated and amplified in Huh7 cells. The viruses in the conditioned medium were harvested and clarified by centrifugation and stored at −80 °C.

Luciferase assay

HEK293T cells were seeded in 12-well plates and transfected with the pIFN-β promoter or pISRE promoter, pRL-CMV, and p3 ×Flag-DHCR24 by using Lipofectamine 2000 (Lipo2000; Thermo Fisher Scientific). The reporter gene activities were measured using a dual-Luciferase reporter assay, according to the manufacturer's instructions (Promega).

Real-time PCR assay

Total cellular RNA was isolated using TRIzol Reagent (Invitrogen). The superscript III first-strand synthesis kit for reverse transcription of RNA was purchased from Invitrogen. After RQ1 DNase (Promega) treatment, the extracted RNA was used as the template for RT-PCR. Real-time PCR was performed as described previously (37). GAPDH was used as the internal control. The primers used for real-time PCR are listed in Table 1.

ELISA

Concentrations of IFN-β in the cell supernatants or mouse serum were measured by ELISA commercial kits (BBI) according to the manufacturer's instructions. Briefly, added 100 µL standards or test samples to each reaction well and incubated for 90 min at 37°C

TABLE 1 Primers for real-time PCR

Primer designation	Primer sequence
Human-*GAPDH* (F)	5′-AATGGGCAGCCGTTAGGAAA-3′
Human-*GAPDH* (R)	5′-GCGCCCAATACGACCAAATC-3′
Human-*DHCR24* (F)	5′- GACCTCCATTGGCTGGACTC-3′
Human-*DHCR24* (R)	5′- GGTCTGAGTTTTCGGACGGA-3′
Human-*IFNβ* (F)	5′-CAGCATTTTCAGTGTCAGAAGC-3′
Human-*IFNβ* (R)	5′-TCATCCTGTCCTTGAGGCAGT-3′
Human-*IL28A* (F)	5′-GCCTCAGAGTTTCTTCTGC-3′
Human-*IL28A* (R)	5′-AAGGCATCTTTGGCCCTCTT-3′
Human-*IL29* (F)	5′-CGCCTTGGAAGAGTCACTCA-3′
Human-*IL29* (R)	5′-GAAGCCTCAGGTCCCAATTC-3′
Human-*ISG15* (F)	5′-CACCGTGTTCATGAATCTGC-3′
Human-*ISG15* (R)	5′-CTTTATTTCCGGCCCTTGAT-3′
Human-*MX1* (F)	5′-CAACCTGTGCAGCCAGTATGA-3′
Human-*MX1* (R)	5′-AGCCCGCAGGGAGTCAAT-3′
Human-*IFITM1* (F)	5′-CGGCTCTGTGACAGTCTACC-3′
Human-*IFITM1* (R)	5′-CTGCTGTATCTAGGGGCAGG-3′
Human-*IRF3* (F)	5′-AAGAGTGGGAGTTCGAGGTG-3′
Human-*IRF3* (R)	5′-TCACGTAGCTCATCACTCCC-3′
Human-*MAVS* (F)	5′-AGCAAGAGACCAGGATCGAC-3′
Human-*MAVS* (R)	5′-ATGAAGTACTCCACCCAGCC-3′
Human-*TRIM21* (F)	5′-CCCCTCTAACCCTCTGTCCA-3′
Human-*TRIM21* (R)	5′-GGGGAAAAGAGGCAGGGTTT-3′
Mouse-*Gapdh* (F)	5′-CAGGAGAGTGTTTCCTCGTCC-3′
Mouse-*Gapdh* (R)	5′-TGTCAGATGCCGCAGTTCTT-3′
Mouse-*Ifnb* (F)	5′-CGTGGGAGATGTCCTCAACT-3′
Mouse-*Ifnb* (R)	5′-AGATCTCTGCTCGGACCACC-3′
VSV (F)	5′-CAAGTCAAAATGCCCAAGAGTCACA-3′
VSV (R)	5′-TTTCCTTGCATTGTTCTACAGATGG-3′

after sealing the plate. Discarded the liquid and dry it, add 100 µL biotin-conjugated antibody working solution to each reaction well, and incubated for 60 min at 37°C. Discarded the liquid and dry it, added 350 µL washing solution to each reaction well, and repeated four times. Added 100 µL HRP-conjugated streptavidin working solution to each reaction well and incubated for 30 min at 37°C. Added 300 µL washing solution to each reaction well and repeated four times. Added 90 µL Substrate reagent (Hiding from light) to each reaction well, and the color was developed at 37°C for about 15 min. Added 50 µL stop solution to each reaction well and immediately measured the OD value at a wavelength of 450 nm with a microplate reader (within 5 min).

Western blotting

Cells were washed with phosphate-buffered saline (PBS) and lysed with RIPA buffer (Thermo Fisher Scientific) supplemented with 1% protease and phosphatase inhibitor cocktail (TargetMol, USA). The lysates were incubated on ice for 30 min and centrifuged at 16,000 × *g* for 15 min at 4°C. Protein concentration was determined using BCA kits (Dojindo). Proteins were resolved on sodium dodecyl sulfate-polyacrylamide gel electrophoresis (SDS-PAGE) gels with running buffer (Tris 3.0 g, Glycine 14.4 g, SDS 1.0 g, and ddH_2O 1.0 L), first 80 V for 30 min, then 120 V for 1–2 h, and transferred to polyvinylidene difluoride (PVDF) membranes (Millipore) with transfer buffer (Tris 3.03 g, Glycine 14.4 g, ddH_2O 800 mL, and methanol 200 mL), 100 V for 2 h. The PVDF membranes were then blocked with 5% skim milk for 2 h and sequentially incubated with primary and secondary antibodies. The bound antibodies were detected using SuperSignal West Pico chemiluminescent substrate (Pierce, Rockford, IL).

Co-IP and immunoblotting

Cells were washed with PBS and lysed with IP buffer (Thermo Fisher Scientific) supplemented with 1% protease and phosphatase inhibitor cocktail (TargetMol, USA). The lysates were incubated on ice for 30 min and centrifuged at 16,000 × *g* for 15 min at 4°C. Protein concentration was determined using BCA kits (Dojindo). The cell lysates (400 µg) were supplemented with PBS to 200 µL and incubated with IgG or the indicated antibodies overnight. Then crosslinked to 30 µL of Protein G Agarose (Millipore) for 6 h. After spinning down and washing five times with PBS, the immunocomplexes were resuspended in SDS sample buffer for analysis by SDS-PAGE.

Cell counting kit-8 assay

Equal numbers of viable cells were plated in 96-well plates, and the culture plates were pre-cultured in a cell incubator for 24 h. Then removed the medium, added 100 µL U18666A supplemented medium, and treated with DMSO at 0.1%. Incubated the culture plates in the incubator for a period of time, such as 0, 24, 48, and 72 h. Added 10 µL CCK-8 (Dojindo) to each well and be careful not to create bubbles in the well. Incubated the culture plates in the incubator for 1–4 h, and optical density was recorded at 450 nm.

Serum cholesterol

The concentration of serum cholesterol was measured with a cholesterol determination kit (Sigma-Aldrich, MAK043). Briefly, the serum samples (0.5–5 µL/well) were first added directly to the 96-well flat-bottom clear plates. Then set up the reaction mixes, including 44 µL cholesterol assay, 2 µL cholesterol probe, 2 µL cholesterol enzyme mix, and 2 µL cholesterol esterase, and added 50 µL of the appropriate reaction mix to each of the wells. Mixed well using a horizontal shaker or by pipetting and incubated the reaction for 1 h at 37 °C. Protect the plate from light during the incubation. For colorimetric assays, measured the absorbance at 570 nm.

Plaque assay

The supernatants of HLCZ01 and the homogenates of livers from infected mice were used to infect monolayers of Vero cells. One hour later, the infected cells were washed with PBS three times followed by incubation with complete medium containing 2% agarose for 24 h. The cells were fixed with 4% paraformaldehyde for 30 min and stained with 1% crystal violet for 30 min before counting the plaques.

ACKNOWLEDGMENTS

We would like to thank Xuetao Cao for VSV and HSV-1. We also appreciate Chen Liu, Hongbing Shu, Zhengfan Jiang, and Yang Xiao for kindly sharing research materials.

This work was supported by National Natural Science Foundation of China (82072269 and 81730064 to HZ) and National Major Science and Technology Projects of China (2017ZX10202201-005) to H.Z. and the Postgraduate Scientific Research Innovation Project of Hunan Province (CX20220385) to Q.L.

AUTHOR AFFILIATIONS

[1]Institute of Pathogen Biology and Immunology, College of Biology, State Key Laboratory of Chemo/Biosensing and Chemometrics, Hunan University, Changsha, China
[2]Department of Pathogen Biology and Immunology, Key Laboratory of Tropical Translational Medicine of Ministry of Education, Institute of Pathogen Biology and Immunology, School of Basic Medicine and Life Science, The University of Hong Kong Joint Laboratory of Tropical Infectious Diseases, Hainan Medical University, Hainan, China
[3]Department of Clinical Laboratory of the Second Affiliated Hospital of Hainan Medical University, Hainan Medical University, Hainan, China

AUTHOR ORCIDs

Haizhen Zhu http://orcid.org/0000-0001-5926-6186

FUNDING

Funder	Grant(s)	Author(s)
MOST | National Natural Science Foundation of China (NSFC)	82072269	Haizhen Zhu
MOST | National Natural Science Foundation of China (NSFC)	81730064	Haizhen Zhu
MOST | National Major Science and Technology Projects of China (National Major Science and Technology Project of China)	2017ZX10202201-005	Haizhen Zhu
Hunan Provincial Innovation Foundation for Postgraduate	CX20220385	Qian Liu

AUTHOR CONTRIBUTIONS

Qian Liu, Conceptualization, Data curation, Formal analysis, Funding acquisition, Investigation, Methodology, Project administration, Resources, Software, Supervision, Validation, Visualization, Writing – original draft, Writing – review and editing | Shengwen Chen, Investigation, Methodology, Project administration | Renyun Tian, Methodology | Binbin Xue, Resources | Huiyi Li, Validation | Mengmeng Guo, Methodology | Shun Liu, Methodology | Ming Yan, Methodology | Ruina You, Validation | Luoling Wang, Methodology | Di Yang, Validation | Mengyu Wan, Validation.

ADDITIONAL FILES

The following material is available online.

Supplemental Material

Table S1 (JVI01513-23-s0001.xls). RNAseq data of HLCZ01 cells, with or without VSV infection.

REFERENCES

1. Tall AR, Yvan-Charvet L. 2015. Cholesterol, inflammation and innate immunity. Nat Rev Immunol 15:104–116. https://doi.org/10.1038/nri3793
2. Reboldi A, Dang E. 2018. Cholesterol metabolism in innate and adaptive response. F1000Res 7:F1000 Faculty Rev-1647. https://doi.org/10.12688/f1000research.15500.1
3. Liu S-Y, Aliyari R, Chikere K, Li G, Marsden MD, Smith JK, Pernet O, Guo H, Nusbaum R, Zack JA, Freiberg AN, Su L, Lee B, Cheng G. 2013. Interferon-inducible cholesterol-25-hydroxylase broadly inhibits viral entry by production of 25-hydroxycholesterol. Immunity 38:92–105. https://doi.org/10.1016/j.immuni.2012.11.005
4. York AG, Williams KJ, Argus JP, Zhou QD, Brar G, Vergnes L, Gray EE, Zhen A, Wu NC, Yamada DH, Cunningham CR, Tarling EJ, Wilks MQ, Casero D, Gray DH, Yu AK, Wang ES, Brooks DG, Sun R, Kitchen SG, Wu T-T, Reue K, Stetson DB, Bensinger SJ. 2015. Limiting cholesterol biosynthetic flux spontaneously engages type I IFN signaling. Cell 163:1716–1729. https://doi.org/10.1016/j.cell.2015.11.045
5. Xiao J, Li W, Zheng X, Qi L, Wang H, Zhang C, Wan X, Zheng Y, Zhong R, Zhou X, Lu Y, Li Z, Qiu Y, Liu C, Zhang F, Zhang Y, Xu X, Yang Z, Chen H, Zhai Q, Wei B, Wang H. 2020. Targeting 7-dehydrocholesterol reductase integrates cholesterol metabolism and Irf3 activation to eliminate infection. Immunity 52:109–122. https://doi.org/10.1016/j.immuni.2019.11.015
6. Wang Y, Wang Y, Ding L, Ren X, Wang B, Wang L, Zhao S, Yue X, Wu Z, Li C, Liang X, Ma C, Gao L. 2022. Tim-4 reprograms cholesterol metabolism to suppress antiviral innate immunity by disturbing the Insig1-SCAP interaction in Macrophages. Cell Rep 41:111738. https://doi.org/10.1016/j.celrep.2022.111738
7. Chan YK, Gack MU. 2015. RIG-I-like receptor regulation in virus infection and immunity. Curr Opin Virol 12:7–14. https://doi.org/10.1016/j.coviro.2015.01.004
8. Rehwinkel J, Gack MU. 2020. RIG-I-like receptors: their regulation and roles in RNA sensing. Nat Rev Immunol 20:537–551. https://doi.org/10.1038/s41577-020-0288-3
9. Onomoto K, Onoguchi K, Yoneyama M. 2021. Regulation of RIG-I-like receptor-mediated signaling: Interaction between host and viral factors. Cell Mol Immunol 18:539–555. https://doi.org/10.1038/s41423-020-00602-7
10. Hou F, Sun L, Zheng H, Skaug B, Jiang Q-X, Chen ZJ. 2011. MAVS forms functional prion-like aggregates to activate and propagate antiviral innate immune response. Cell 146:448–461. https://doi.org/10.1016/j.cell.2011.06.041
11. Sharma A, Kontodimas K, Bosmann M. 2021. The MAVS immune recognition pathway in viral infection and sepsis. Antioxid Redox Sign 35:1376–1392. https://doi.org/10.1089/ars.2021.0167
12. Vazquez C, Horner SM. 2015. MAVS coordination of antiviral innate immunity. J Virol 89:6974–6977. https://doi.org/10.1128/JVI.01918-14
13. Cai X, Chen ZJ. 2014. Prion-like polymerization as a signaling mechanism. Trends Immunol 35:622–630. https://doi.org/10.1016/j.it.2014.10.003

14. Seth RB, Sun L, Chen ZJ. 2006. Antiviral innate immunity pathways. Cell Res 16:141–147. https://doi.org/10.1038/sj.cr.7310019
15. Motwani M, Pesiridis S, Fitzgerald KA. 2019. DNA sensing by the cGAS-STING pathway in health and disease. Nat Rev Genet 20:657–674. https://doi.org/10.1038/s41576-019-0151-1
16. Hopfner K-P, Hornung V. 2020. Molecular mechanisms and cellular functions of cGAS-STING signalling. Nat Rev Mol Cell Biol 21:501–521. https://doi.org/10.1038/s41580-020-0244-x
17. Zhang X, Bai X-C, Chen ZJ. 2020. Structures and mechanisms in the cGAS-STING innate immunity pathway. Immunity 53:43–53. https://doi.org/10.1016/j.immuni.2020.05.013
18. Chen Q, Sun L, Chen ZJ. 2016. Regulation and function of the cGAS-STING pathway of cytosolic DNA sensing. Nat Immunol 17:1142–1149. https://doi.org/10.1038/ni.3558
19. Mosallanejad K, Kagan JC. 2022. Control of innate immunity by the cGAS-STING pathway. Immunol Cell Biol 100:409–423. https://doi.org/10.1111/imcb.12555
20. Zerenturk EJ, Sharpe LJ, Ikonen E, Brown AJ. 2013. Desmosterol and DHCR24: unexpected new directions for a terminal step in cholesterol synthesis. Prog Lipid Res 52:666–680. https://doi.org/10.1016/j.plipres.2013.09.002
21. Waterham HR, Koster J, Romeijn GJ, Hennekam RCM, Vreken P, Andersson HC, FitzPatrick DR, Kelley R, Wanders RJA. 2001. Mutations in the 3beta-hydroxysterol Delta24-reductase gene cause desmosterolosis, an autosomal recessive disorder of cholesterol biosynthesis. Am J Hum Genet 69:685–694. https://doi.org/10.1086/323473
22. Wechsler A, Brafman A, Shafir M, Heverin M, Gottlieb H, Damari G, Gozlan-Kelner S, Spivak I, Moshkin O, Fridman E, Becker Y, Skaliter R, Einat P, Faerman A, Björkhem I, Feinstein E. 2003. Generation of viable cholesterol-free mice. Science 302:2087–2087. https://doi.org/10.1126/science.1090776
23. Greeve I, Hermans-Borgmeyer I, Brellinger C, Kasper D, Gomez-Isla T, Behl C, Levkau B, Nitsch RM. 2000. The human DIMINUTO/DWARF1 homolog seladin-1 confers resistance to Alzheimer's disease-associated neurodegeneration and oxidative stress. J Neurosci 20:7345–7352. https://doi.org/10.1523/JNEUROSCI.20-19-07345.2000
24. Bai X, Mai M, Yao K, Zhang M, Huang Y, Zhang W, Guo X, Xu Y, Zhang Y, Qurban A, Duan L, Bu J, Zhang J, Wu J, Zhao Y, Yuan X, Zu H. 2022. The role of DHCR24 in the pathogenesis of AD: re-cognition of the relationship between cholesterol and AD pathogenesis. Acta Neuropathol Commun 10:35. https://doi.org/10.1186/s40478-022-01338-3
25. Bai X, Wu J, Zhang M, Xu Y, Duan L, Yao K, Zhang J, Bo J, Zhao Y, Xu G, Zu H. 2021. DHCR24 knock-down induced Tau hyperphosphorylation at Thr181, Ser199, Thr231, Ser262, Ser396 epitopes and inhibition of autophagy by overactivation of GSK3beta/mTOR signaling. Front Aging Neurosci 13:513605. https://doi.org/10.3389/fnagi.2021.513605
26. Wu C, Miloslavskaya I, Demontis S, Maestro R, Galaktionov K. 2004. Regulation of cellular response to oncogenic and oxidative stress by seladin-1. Nature 432:640–645. https://doi.org/10.1038/nature03173
27. Shen Y, Zhou J, Nie K, Cheng S, Chen Z, Wang W, Wei W, Jiang D, Peng Z, Ren Y, Zhang Y, Fan Q, Richards KL, Qi Y, Cheng J, Tam W, Ma J. 2022. Oncogenic role of the SOX9-DHCR24-cholesterol biosynthesis axis in IGH-BCL2+ diffuse large B-cell lymphomas. Blood 139:73–86. https://doi.org/10.1182/blood.2021012327
28. Liu X-P, Yin X-H, Meng X-Y, Yan X-H, Cao Y, Zeng X-T, Wang X-H. 2018. DHCR24 predicts poor clinicopathological features of patients with bladder cancer: a STROBE-compliant study. Medicine (Baltimore) 97:e11830. https://doi.org/10.1097/MD.0000000000011830
29. Horvat S, McWhir J, Rozman D. 2011. Defects in cholesterol synthesis genes in mouse and in humans: lessons for drug development and safer treatments. Drug Metab Rev 43:69–90. https://doi.org/10.3109/03602532.2010.540580
30. Yang D, Zuo C, Wang X, Meng X, Xue B, Liu N, Yu R, Qin Y, Gao Y, Wang Q, Hu J, Wang L, Zhou Z, Liu B, Tan D, Guan Y, Zhu H. 2014. Complete replication of hepatitis B virus and hepatitis C virus in a newly developed hepatoma cell line. Proc Natl Acad Sci U S A 111:E1264–73. https://doi.org/10.1073/pnas.1320071111
31. Takano T, Tsukiyama-Kohara K, Hayashi M, Hirata Y, Satoh M, Tokunaga Y, Tateno C, Hayashi Y, Hishima T, Funata N, Sudoh M, Kohara M. 2011. Augmentation of DHCR24 expression by hepatitis C virus infection facilitates viral replication in hepatocytes. J Hepatol 55:512–521. https://doi.org/10.1016/j.jhep.2010.12.011
32. Quan X, Chen X, Sun D, Xu B, Zhao L, Shi X, Liu H, Gao B, Lu X. 2016. The mechanism of the effect of U18666A on blocking the activity of 3beta-hydroxysterol Delta-24-reductase (DHCR24): molecular dynamics simulation study and free energy analysis. J Mol Model 22:46. https://doi.org/10.1007/s00894-016-2907-2
33. Tian K-Y, Chang H-M, Wang J, Qi M-H, Wang W-L, Qiu Y, Liang K, Chen F-Q, Zha D-J, Qiu J-H. 2019. Inhibition of DHCR24 increases the cisplatin-induced damage to cochlear hair cells *in vitro*. Neurosci Lett 706:99–104. https://doi.org/10.1016/j.neulet.2019.05.019
34. Ren Z, Ding T, Zuo Z, Xu Z, Deng J, Wei Z. 2020. Regulation of MAVS expression and signaling function in the antiviral innate immune response. Front Immunol 11:1030. https://doi.org/10.3389/fimmu.2020.01030
35. Liu B, Zhang M, Chu H, Zhang H, Wu H, Song G, Wang P, Zhao K, Hou J, Wang X, Zhang L, Gao C. 2017. The ubiquitin E3 ligase TRIM31 promotes aggregation and activation of the signaling adaptor MAVS through Lys63-linked polyubiquitination. Nat Immunol 18:214–224. https://doi.org/10.1038/ni.3641
36. Chen S, Liu Q, Zhang L, Ma J, Xue B, Li H, Deng R, Guo M, Xu Y, Tian R, Wang J, Cao W, Yang Q, Wang L, Li X, Liu S, Yang D, Zhu H. 2022. The role of REC8 in the innate immune response to viral infection. J Virol 96:e0217521. https://doi.org/10.1128/jvi.02175-21
37. Xue B, Li H, Guo M, Wang J, Xu Y, Zou X, Deng R, Li G, Zhu H, Ou J-HJ. 2018. TRIM21 promotes innate immune response to RNA viral infection through Lys27-linked polyubiquitination of MAVS. J Virol 92:14. https://doi.org/10.1128/JVI.00321-18
38. Wang Q, Liu X, Cui Y, Tang Y, Chen W, Li S, Yu H, Pan Y, Wang C. 2014. The E3 ubiquitin ligase AMFR and INSIG1 bridge the activation of TBK1 kinase by modifying the adaptor STING. Immunity 41:919–933. https://doi.org/10.1016/j.immuni.2014.11.011
39. Mirza R, Hayasaka S, Takagishi Y, Kambe F, Ohmori S, Maki K, Yamamoto M, Murakami K, Kaji T, Zadworny D, Murata Y, Seo H. 2006. DHCR24 gene knockout mice demonstrate lethal dermopathy with differentiation and maturation defects in the epidermis. J Invest Dermatol 126:638–647. https://doi.org/10.1038/sj.jid.5700111
40. van Diepen JA, Berbée JFP, Havekes LM, Rensen PCN. 2013. Interactions between inflammation and lipid metabolism: relevance for efficacy of anti-inflammatory drugs in the treatment of atherosclerosis. Atherosclerosis 228:306–315. https://doi.org/10.1016/j.atherosclerosis.2013.02.028
41. DeBose-Boyd RA. 2018. Significance and regulation of lipid metabolism. Semin Cell Dev Biol 81:97. https://doi.org/10.1016/j.semcdb.2017.12.003
42. Zhang Z, Fang X, Wu X, Ling L, Chu F, Li J, Wang S, Zang J, Zhang B, Ye S, Zhang L, Yang B, Lin S, Huang H, Wang A, Zhou F. 2020. Acetylation-dependent deubiquitinase OTUD3 controls MAVS activation in innate antiviral immunity. Molecular Cell 79:304–319. https://doi.org/10.1016/j.molcel.2020.06.020
43. Zhang Z-D, Xiong T-C, Yao S-Q, Wei M-C, Chen M, Lin D, Zhong B. 2020. RNF115 plays dual roles in innate antiviral responses by catalyzing distinct ubiquitination of MAVS and MITA. Nat Commun 11:5536. https://doi.org/10.1038/s41467-020-19318-3
44. Sun H, Zhang Q, Jing Y-Y, Zhang M, Wang H-Y, Cai Z, Liuyu T, Zhang Z-D, Xiong T-C, Wu Y, Zhu Q-Y, Yao J, Shu H-B, Lin D, Zhong B. 2017. USP13 negatively regulates antiviral responses by deubiquitinating STING. Nat Commun 8:15534. https://doi.org/10.1038/ncomms15534
45. Kallin A, Johannessen LE, Cani PD, Marbehant CY, Essaghir A, Foufelle F, Ferré P, Heldin C-H, Delzenne NM, Demoulin J-B. 2007. SREBP-1 regulates the expression of heme oxygenase 1 and the phosphatidylinositol-3 kinase regulatory subunit p55 gamma. J Lipid Res 48:1628–1636. https://doi.org/10.1194/jlr.M700136-JLR200
46. Demoulin J-B, Ericsson J, Kallin A, Rorsman C, Rönnstrand L, Heldin C-H. 2004. Platelet-derived growth factor stimulates membrane lipid synthesis through activation of phosphatidylinositol 3-kinase and sterol regulatory element-binding proteins. J Biol Chem 279:35392–35402. https://doi.org/10.1074/jbc.M405924200